

DOI: <https://dx.doi.org/10.21123/bsj.2023.7748>

Synthesis, Characterization and Theoretical Investigation of Innovative Charge-transfer Complexes Derived from the N-phenyl 3,4-selenadiazobenzophenone Imine

Haider Shanshool Mohammed 

Nuha Hussain Al-Saadawy* 

Department of Chemistry, College of Science, University of Thi-Qar, Muthanna, Iraq.

*Corresponding author: haider.shanshool@mu.edu.iq

E-mail address: Nuh.hussain@sci.utq.edu.iq

Received 13/9/2022, Revised 8/11/2022, Accepted 9/11/2022, Published Online First 20/3/2023,
Published 28/10/2023



This work is licensed under a [Creative Commons Attribution 4.0 International License](https://creativecommons.org/licenses/by/4.0/).

Abstract:

In the current study, a direct method was used to create a new series of charge-transfer complexes of chemicals. In a good yield, new charge-transfer complexes were produced when different quinones reacted with acetonitrile as solvent in a 1:1 mole ratio with N-phenyl-3,4-selenadiazobenzophenone imine. By using analysis techniques like UV, IR, and ^1H , ^{13}C -NMR, every substance was recognized. The analysis's results matched the chemical structures proposed for the synthesized substances. Functional theory of density (DFT) has been used to analyze the molecular structure of the produced Charge-Transfer Complexes, and the energy gap, HOMO surfaces, and LUMO surfaces have all been created throughout the geometry optimization process utilizing the base set of 3-21G geometrical structures. The molecular geometry and contours for compounds with charge-transfer complexes have been evaluated during the process of geometrical optimization. By investigating the interactions between donor and acceptor, we have also been contrasting the energies (HOMO energies) of the chemicals in charge-transfer complexes. For molecules containing charge-transfer complexes, the lower case, electronegativity, ionization potential, electron affinity, and electrophilicity have all been calculated and studied.

Keywords: Charge-transfer Complexes, Different quinones, Energy gap, HOMO energies, N-phenyl 3,4-selenadiazobenzophenone imine.

Introduction:

Organic complexes of charge-transfer consist of two systems formed by a pair of electrons with a specified stoichiometry- an electron donor and an electron acceptor unit. For many years, charge-transfer complexes have been thoroughly studied in an attempt to develop standards for creating materials with high room-temperature mobility or superconductivity ¹. However, in recent years, attention has also been given to the creation of more technologically advanced applications utilizing such charge-transfer complexes ²⁻⁴. As an example, ferroelectrics ⁵, photoconductors ^{6,7}, light detectors ⁸, strain sensors ⁹, thermoelectric ¹⁰, transistors of organic field-effect (OFETs), where CT complexes can function as organic metals ^{11,12} or organic semiconductors ^{13,14}. Organoselenium compounds have long been demonstrated to be particularly significant chemicals from a practical standpoint, in

addition to being useful intermediate products in organic synthesis and realistic models for exploring fundamental difficulties of theoretical chemistry ¹⁵⁻¹⁸. Organoselenium compounds' unusual properties make them ideal as synthons because selenium-containing fragments can be easily incorporated into organic compounds and selenium atoms can be eliminated through appropriate processes, such as oxidation, which results in the formation of a double bond through synelimination of selenium oxide ¹⁹. The majority of the reactions used to synthesis organo compounds of selenadiazole are known to be based on the interaction between organo diamine and selenium dioxide ²⁰⁻²². This study's objective is to synthesize new charge-transfer complexes by reacting five types of quinones (p-benzoquinone, p-anthraquinone, Tetrachloro benzoquinone (TCBQ), 7, 7, 8, 8-Tetracyano quino dimethane, 1,4-

Dihydroxyanthraquinon). With N-phenyl 3,4-selenadiazobenzophenone imine, to create new charge-transfer complexes compound.

Material and Methods:

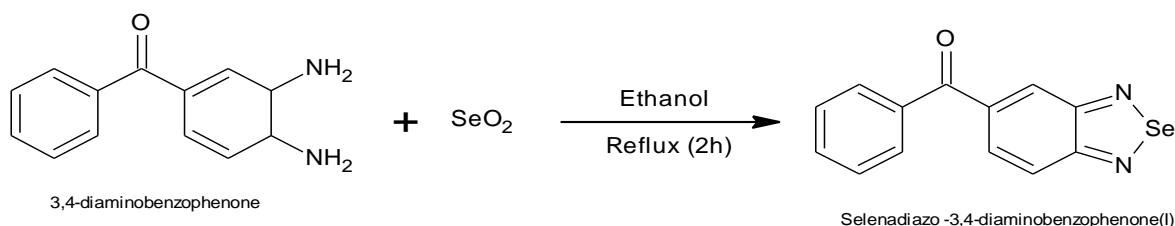
Materials

The chemicals used included 3,4-diaminobenzophenone (Fluka), aniline (Sigma-Aldrich), ethanol absolute and acetonitrile (Fluka.), p-benzoquinone (Sigma-Aldrich), anthraquinone (Sigma-Aldrich), Tetrachloro benzoquinone (Sigma-Aldrich), 7,7,8,8-Tetracyanoquinodimethane (Fluka.), 1,4-Dihydroxyanthraquinon (Strem chemicals Inc.), selenium dioxide powder (Strem chemicals Inc.), nitric acid (HGB).

Computational Analysis Program: Gaussian 09W set of (3-21G) basis and using estimated DFT-based descriptors.

Instrumental

Shimadzu UV-visible Spectrophotometer double-beam model UV-1650 (Japan) equipped quartz (cells 1.00 cm), Electro thermal (melting point) apparatus. ¹H-NMR spectra were recorded on (Bruker 500 MHz spectrometers) with TMS as an inner reference utilizing soluble DMSO-d₆. Infrared spectra When using KBr, the range of wave numbers is 4000-400 Cm⁻¹ utilizing an FT-IR spectrophotometer, Shimadzu model 8400 S.



Scheme 1. Preparation of 3,4-Selenadiazobenzophenone(I)

2. Preparation of N-phenyl 3,4-selenadiazobenzophenone Imine (II)

An amount of 0.279 g (3 mmol) of pure aniline was dissolved in 20 ml of ethanol and mixed with 0.860 g (3 mmol) of Selenadiazobenzophenone (prepared in first step) dissolved in 20 ml of ethanol also. By using a round bottom flask, the mixture was refluxed in a water bath for 5 hours. After that, the solution was cooled, washed with cool ethanol, and filtered with a Buechner funnel to obtain a light coffee-colored precipitate with a yield of 74% and a melting point 105–110 C°. Rf value=0.93 (7: 3) (Ethyl acetate\nhexane UV-visible spectra were recorded at 200-750 nm in solvent of DMSO, n-π* and π-π* are two different types of electronic transitions with λ max

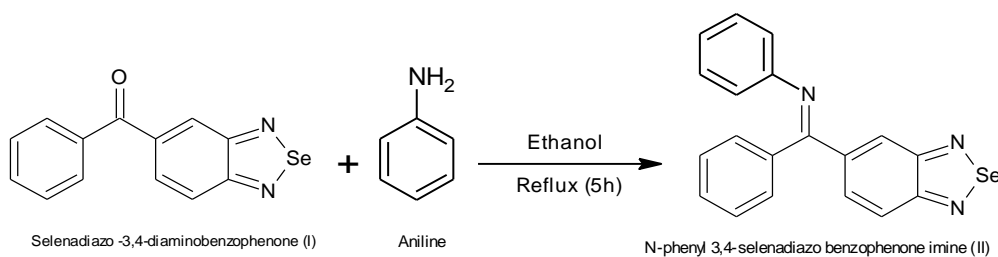
Procedure

1. Preparation of 3,4-Selenadiazobenzophenone(I)

An amount of (20 mmol) 4.24 g of 3,4-diaminobenzophenone was dissolved in (30 ml) of ethanol and mixed with (20 mmol) 2.2 g of selenium dioxide dissolved in 30 ml of ethanol. By using a round bottom flask, the mixture was refluxed in a water bath for 2 hours until a coffee-colored solution is formed. After that, the cooled solution was then filtered and washed with hot ethanol to obtain a coffee-colored precipitate with an 80% yield and an M.P (melting point) of 95°C. Rf value=0.78 (7:3) (Ethyl acetate\nhexane). UV-visible spectra were recorded at 200-750 nm in solvent of DMSO, n-π* and π-π* are two different types of electronic transitions. with λ max 225 nm, 273 nm, 355 nm. FT-IR with KBr disk: ν(C-H) Ar. = 3061 cm⁻¹, ν(C=O) Ar. = 1649 cm⁻¹, ν(C=N) Ar. = 1579-1600 cm⁻¹, ν(C=C) Ar.= 1490-1500 cm⁻¹, ν (C-Se-N) Ar. = 3260 cm⁻¹; Signals of ¹H-NMR (500 MHz-DMSO-d₆) δ Ar. ¹⁴C-H, ¹⁶C-H (2H, m, δ 7.52); Ar. ¹⁵C-H, ¹⁷C-H (2H, m, δ 7.74); Ar. ¹³C-H, (1H, t, δ 7.89); Ar. ⁹C-H, (1H, d, δ 7.90); Ar. ⁸C-H, (1H, d, δ 8.02); Ar. ⁶C-H, (1H, s, δ 8.11). ¹³C NMR: Ar. ⁶C δ 126.7 (1C, s), Ar. ⁹C 127.2 (1C, s), Ar. ¹⁵C 127.8 (1C, s), Ar. ⁸C 127.9 (1C, s), Ar. (¹⁴C, ¹⁶C) 128.4 (2C, s), Ar. (¹³C, ¹⁷C) 129.0 (2C, s), Ar. ⁷C 129.3 (1C, s), Ar. ¹²C 137.2 (1C, s), Ar. (³C, ⁴C) 160.4-160.6 (2C, 160.5 (s), 160.5 (s)), Ar. ¹⁰C 195.0 (1C, s). As shown in Scheme 1, Table 1,2 and 3, Figs.1, 8, 15 and 22.

(220 nm, 233 nm, 240 nm, 243 nm, 250 nm, 270 nm, 345 nm). FT-IR with KBr disk: ν(C-H) Ar. = 3063 cm⁻¹, ν(C=N) Ar. = (1593-1637) cm⁻¹, ν(C=C) Ar. = 1448-1556 cm⁻¹, ν(C-N) Ar. = 1325 cm⁻¹, ν (C-Se-N) Ar. = 3250 cm⁻¹; Signals of ¹H-NMR (500 MHz-DMSO-d₆) δ Ar. ¹³C-H, ¹⁴C-H, ¹⁵C-H, ¹⁶C-H, ¹⁷C-H, ²⁰C-H, ²¹C-H, ²²C-H (8H, m, δ 7.5-7.7); Ar. ¹⁹C-H, ²³C-H (2H, m, δ 8.2); Ar. ⁹C-H, (1H, d, δ 8.01); Ar. ⁸C-H, (1H, d, δ 8.03); Ar. ⁶C-H, (1H, s, δ 8.10); ¹³C NMR: Ar. ⁶C δ 126.6 (1C, s), Ar. ⁹C 128.6 (1C, s), Ar. (¹³C, ¹⁷C) 124.1 (2C, s), Ar. ⁸C 129.1 (1C, s), Ar. (¹⁴C, ¹⁶C) 130.1 (2C, s), Ar. ¹⁵C δ 127.8 (1C, s), Ar. ¹⁸C δ 132.1 (1C, s), Ar. (¹⁹C, ²³C) 129.2 (2C, s), Ar. (²⁰C, ²²C) 128.4 (2C, s), Ar. ²¹C δ 127.8 (1C, s), Ar. ⁷C 127.3 (1C, s), Ar. ¹⁰C 159.1(1C, s), Ar. (³C, ⁴C) 160.5 (2C, 160.5 (s), 160.5 (s)), Ar. ¹²C 138.0 (1C,

s). As shown in Scheme 2, Table 1,2 and 3, Figs.2, 9, 16 and 23.



Scheme 2. Preparation of N-phenyl 3,4-selenadiazobenzophenone Imine (II)

3. Preparing p-Benzoquino N-phenyl 3,4-selenadiazobenzophenone Imine (III)

An amount of (2 mmol) 0.725 g of N-phenyl 3,4-selenadiazobenzophenone imine was dissolved in 30 mL of acetonitrile and mixed with (2 mmol) 0.216 g of p-benzoquinone dissolved in 30 ml of acetonitrile and heated using reflux in a water bath for 3 hours. The solution was cooled and evaporated by a rotary evaporator and washed with small amounts of acetonitrile to obtain a pure and shiny brown crystal precipitate with an 76% yield and an M.P (melting point) of 107°C. Rf value=0.92 (7:3) (Ethyl acetate/n-hexane). UV-visible spectra were recorded at (200-750) nm in solvent of DMSO, $n-\pi^*$ and $\pi-\pi^*$ are two different types of electronic transitions with λ max 205 nm, 230 nm, 236 nm, 270 nm, 280 nm, 355 nm. FT-IR with KBr disk: $\nu(\text{C-H})$ Ar. =3063 cm^{-1} , $\nu(\text{C=O})$ Ar. = 1724-1788 cm^{-1} , $\nu(\text{C=N})$ Ar. = 1597-1639 cm^{-1} , $\nu(\text{C=C})$ Ar. = 1504-1575 cm^{-1} , $\nu(\text{C-N})$ Ar. =1325 cm^{-1} , $\nu(\text{C-Se-N})$ Ar. = 3259 cm^{-1} ; Signals of $^1\text{H-NMR}$ (500 MHz-DMSO- d_6) δ Ar. $^{13}\text{C-H}$, $^{15}\text{C-H}$ (2H, m, δ 7.53), δ Ar. $^{15}\text{C-H}$, $^{16}\text{C-H}$ (2H, m, δ 7.58), δ Ar. $^{17}\text{C-H}$, $^{19}\text{C-H}$, $^{20}\text{C-H}$, $^{21}\text{C-H}$, $^{22}\text{C-H}$, (5H, m, δ 7.53 -7.77), δ Ar. $^{25}\text{C-H}$, $^{26}\text{C-H}$, $^{28}\text{C-H}$, $^{29}\text{C-H}$ (4H, m, δ 7.85 -7.90) Ar. $^{23}\text{C-H}$ (1H, d, δ 7.52); Ar. $^9\text{C-H}$, (1H, d, δ 8.01); Ar. $^8\text{C-H}$, (1H, d, δ 8.02); Ar. $^6\text{C-H}$, (1H, s, δ 8.10); as show in Scheme3, Tables.1,2 and 3, Figs.3,10 and 17.

4. Preparing p-Antraquino N-phenyl 3,4-selenadiazobenzophenone Imine (IV)

An amount of (2 mmol) 0.725 g of N-phenyl 3,4-selenadiazobenzophenone imine was dissolved in 30 ml of acetonitrile and mixed with (2 mmol) 0.416 g of anthraquinone dissolved in 30 ml of acetonitrile and heated using reflux in a water bath for 3 hours. The solution was cooled and evaporated by a rotary evaporator and washed with small amounts of acetonitrile to obtain pure and shiny light-yellow crystals precipitate with an 64% yield and an M.P (melting point) of 118-208 °C. Rf value=0.85 (7:3) (Ethyl acetate/n-hexane). UV-visible spectra were recorded at 200-750 nm in solvent of DMSO, $n-\pi^*$ and $\pi-\pi^*$ are two different types of electronic transitions with λ max (215 nm, 230 nm,240 nm, 248

nm, 252 nm, 275 nm, 350 nm). FT-IR with KBr disk: $\nu(\text{C-H})$ Aromatic = 3070 cm^{-1} , $\nu(\text{C=N})$ Aromatic = 1639-1676 cm^{-1} , Ar. $\nu(\text{C=O})$ = 1737-1795 cm^{-1} , $\nu(\text{C=C})$ Aromatic = 1545-1589 cm^{-1} , $\nu(\text{C-N})$ Ar. = 1330 cm^{-1} , Ar. $\nu(\text{C-Se-N})$ = 3319 cm^{-1} ; Signals of $^1\text{H-NMR}$ (500 MHz-DMSO- d_6) δ Ar. $^{13}\text{C-H}$, $^{15}\text{C-H}$ (2H, m, δ 7.58-7.69), δ Ar. $^{14}\text{C-H}$, $^{16}\text{C-H}$ $^{17}\text{C-H}$, (3H, m, δ 7.57-7.63), δ Ar. $^{20}\text{C-H}$, $^{21}\text{C-H}$, $^{19}\text{C-H}$, $^{22}\text{C-H}$, (4H, m, δ 7.57 -7.76), δ Ar. $^{30}\text{C-H}$, $^{31}\text{C-H}$, $^{32}\text{C-H}$, $^{33}\text{C-H}$, $^{34}\text{C-H}$, $^{35}\text{C-H}$, $^{36}\text{C-H}$, $^{37}\text{C-H}$ (8H, m, δ 7.85 -7.95) Ar. $^{23}\text{C-H}$ (1H, d, δ 8.3); Ar. $^9\text{C-H}$, (1H, d, δ 8.26); Ar. $^8\text{C-H}$, (1H, d, δ 8.20); Ar. $^6\text{C-H}$, (1H, s, δ 8.09); as show in Scheme3, Table1,2 and 3, Figures.4,11 and 18.

5. Preparing Tetrachloro Benzoquino N-phenyl 3,4-selenadiazobenzophenone Imine(V)

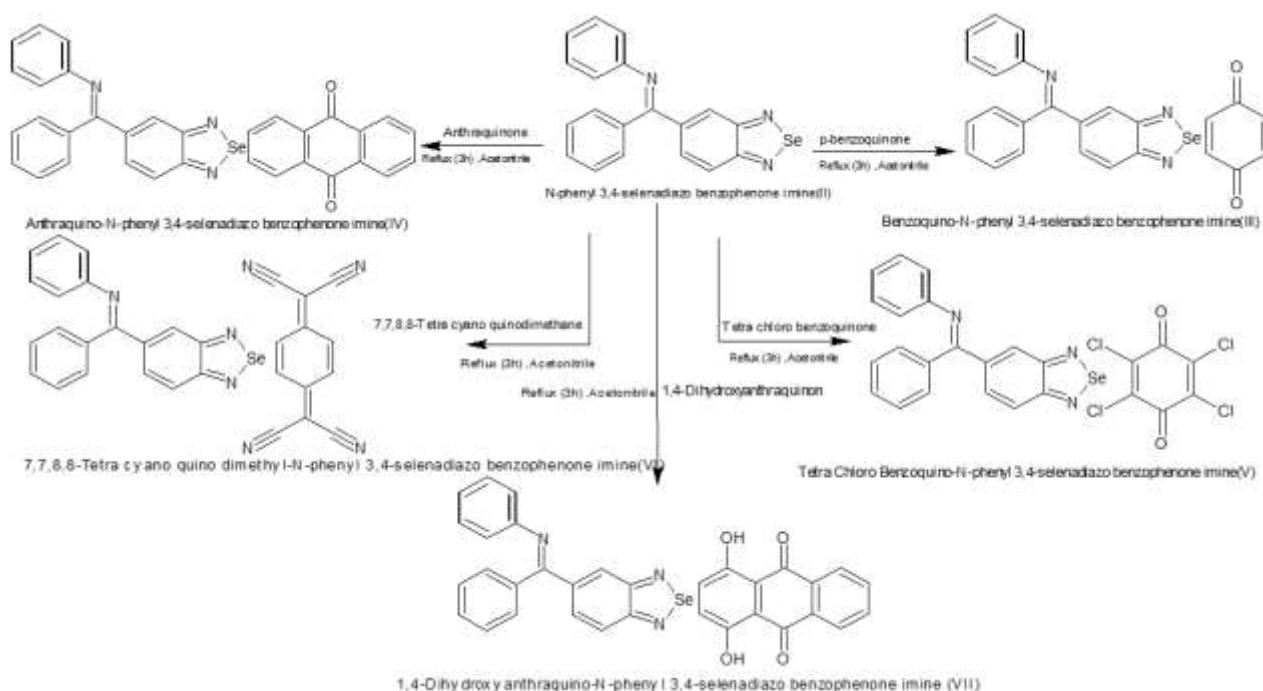
An amount of (2 mmol) 0.725 g of N-phenyl 3,4-selenadiazobenzophenone imine was dissolved in 30 ml of acetonitrile and mixed with (2 mmol) 0.491 g of Tetrachloro benzoquinone dissolved in 30 mL of acetonitrile and heated using reflux in a water bath for 3 hours. The solution was cooled and evaporated by a rotary evaporator and washed with small amounts of acetonitrile to obtain a pure and shiny dark brown crystal crystals precipitate with an 71% yield and an M.P (melting point) of 170-230 °C. Rf value=0.88 (7:3) (Ethyl acetate/n-hexane). UV-visible spectra were recorded at (200-750) nm in solvent of DMSO, $n-\pi^*$ and $\pi-\pi^*$ are two different types of electronic transitions with λ max 215 nm, 237 nm, 240 nm, 248 nm, 285 nm, 350 nm. FT-IR with KBr disk: $\nu(\text{C-H})$ Aromatic = 3063 cm^{-1} , $\nu(\text{C=N})$ Aromatic = 1639-1683 cm^{-1} , $\nu(\text{C=O})$ Aromatic = (1768) cm^{-1} , Ar. $\nu(\text{C=C})$ = 1570-1591 cm^{-1} , $\nu(\text{C-N})$ Ar. = 1325 cm^{-1} , $\nu(\text{C-Se-N})$ Aromatic = 3356 cm^{-1} , $\nu(\text{C-Cl})$ Ar. = 550-880 cm^{-1} ; Signals of $^1\text{H-NMR}$ (500 MHz-DMSO- d_6) were δ Ar. $^{13}\text{C-H}$ (1H, d, δ 8.03), δ Ar. $^{14}\text{C-H}$, $^{15}\text{C-H}$, $^{16}\text{C-H}$ (3H, m, δ 7.86-7.87), δ Ar. $^{17}\text{C-H}$, $^{20}\text{C-H}$, $^{21}\text{C-H}$ (3H, m, δ 7.58-7.77), δ Ar. $^{23}\text{C-H}$ (1H, d, δ 7.62); Ar. $^{19}\text{C-H}$, (1H, d, δ 7.9), $^{22}\text{C-H}$ (1H, t, δ 7.59); Ar. $^9\text{C-H}$, (1H, d, δ 8.02); Ar. $^8\text{C-H}$, (1H, d, δ 8.01); Ar. $^6\text{C-H}$, (1H, s, δ 8.10); as show in Scheme3, Table1,2 and 3, Figners.5, 12 and 19.

6. Preparing 7,7,8,8-Tetracyano Quino Dimethane N-phenyl 3,4-selenadiazobenzophenone Imine (VI)

An amount of (2 mmol) 0.725 g of N-phenyl 3,4-selenadiazobenzophenone imine was dissolved in 30 ml of acetonitrile and mixed with (2 mmol) 0.408 g of 7,7,8,8-Tetracyano quino dimethane dissolved in 30 ml of acetonitrile and heated using reflux in a water bath for 3 hours. The solution was cooled and evaporated by a rotary evaporator and washed with small amounts of acetonitrile to obtain a pure and shiny dark yellow crystal precipitate with an 71% yield and an M.P (melting point) of (149-260) C°. Rf value=0.92 (7:3) (Ethyl acetate/n-hexane). UV-visible spectra were recorded at 200-750 nm in solvent of DMSO, $n-\pi^*$ and $\pi-\pi^*$ are two different types of electronic transitions with λ_{max} 210 nm, 220 nm, 225 nm, 245 nm, 250 nm, 365 nm, 400 nm. FT-IR with KBr disk: $\nu(C-H)$ Aromatic = 3051 cm^{-1} , $\nu(C=N)$ Ar. = (1651-1676) cm^{-1} , $\nu(C=C)$ Ar. = 1541 cm^{-1} , $\nu(C-N)$ Ar. = 1354 cm^{-1} , $\nu(C-Se-N)$ Ar. = 3138 cm^{-1} , $\nu(C\equiv N)$ Ar. = (2222) cm^{-1} ; Signals of ^1H-NMR (500 MHz-DMSO- d_6): δ Ar. $_{13}C-H$, (1H, d, δ 8.01) δ Ar. $_{23}C-H$, $_{14}C-H$ (2H, m, δ 7.86-7.88), δ Ar. $_{15}C-H$, $_{16}C-H$ (2H, m, δ 7.72-7.76), δ Ar. $_{17}C-H$, $_{20}C-H$, $_{21}C-H$, (3H, m, δ 7.86 -7.88), δ Ar. $_{25}C-H$, $_{26}C-H$, $_{28}C-H$, $_{29}C-H$ (4H, m, δ (7.88 -7.89), Ar. $_{22}C-H$, $_{19}C-H$, (2H, t, δ 7.60-7.63); Ar. $_{9}C-H$, (1H, d, δ 8.01); Ar. $_{8}C-H$, (1H, d, δ 8.02); Ar. $_{6}C-H$, (1H, s, δ 8.09); as show in Scheme3, Table1,2 and 3, Figures.6,13 and 20.

7. Preparing 1,4-Dihydroxyanthraquino N-phenyl 3,4-selenadiazobenzophenone Imine (VII)

An amount of (2 mmol) 0.725 g of N-phenyl 3,4-selenadiazobenzophenone imine was dissolved in 30 ml of acetonitrile and mixed with (2 mmol) 0.48 g of 1,4-Dihydroxyanthraquinon dissolved in 30 ml of acetonitrile and heated using reflux in a water bath for 3 hours. The solution was cooled and evaporated by a rotary evaporator and washed with small amounts of acetonitrile to obtain a pure and shiny pink-yellow crystals precipitate with an 70% yield and an M.P (melting point) of 167-187 C°. Rf value=0.88 (7:3) (Ethyl acetate/n-hexane). The UV-visible spectra were recorded at (200-750) nm in solvent of DMSO, $n-\pi^*$ and $\pi-\pi^*$ are two different types of electronic transitions with λ_{max} (210 nm, 225 nm, 230 nm, 245 nm, 255 nm, 273 nm, 335 nm, 473 nm). FT-IR with KBr disk: $\nu(C-H)$ Ar. = 3061 cm^{-1} , $\nu(C=N)$ Ar. = 1629 cm^{-1} , $\nu(C=O)$ Ar.= 1691 cm^{-1} , $\nu(C=C)$ Ar. = (1539-1589) cm^{-1} , $\nu(C-N)$ Ar. = 1357 cm^{-1} , $\nu(C-Se-N)$ Ar.= 3210 cm^{-1} , $\nu(OH)$ Ar. = (3500-3600) cm^{-1} ; Signals of ^1H-NMR (500 MHz-DMSO- d_6): δ Ar. $_{13}C-H$, $_{14}C-H$ (2H, m, δ 7.49-8.02), δ Ar. $_{15}C-H$, $_{16}C-H$ (2H, t, δ 8.02-8.03), Ar. $_{17}C-H$ (1H, s, δ 8.31), δ Ar. $_{21}C-H$, $_{22}C-H$ (2H, t, δ 7.49-8.02), $_{19}C-H$, $_{23}C-H$, (2H, d, δ 7.57 -7.76), δ Ar. $_{27}C-H$, $_{28}C-H$, $_{34}C-H$, $_{35}C-H$, $_{36}C-H$, $_{37}C-H$ (6H, m, δ 8.30 -8.03) Ar. $_{20}C-H$ (1H, d, δ 8.03); Ar. $_{9}C-H$, (1H, d, δ 8.31); Ar. $_{8}C-H$, (1H, d, δ 8.30); Ar. $_{6}C-H$, (1H, s, δ 8.32) δ Ar. $_{39}O-H$, $_{40}O-H$ (2H, s, δ 12.7); as show in Scheme3, Table1,2 and 3, Figures.7,14 and 21.



Scheme 3. Preparation of quino N-phenyl 3,4-selenadiazobenzophenone Imine (compounds III, IV, V, VI, and VII)

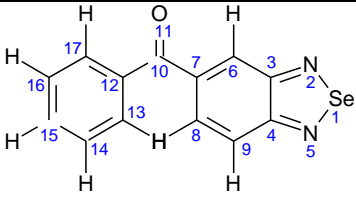
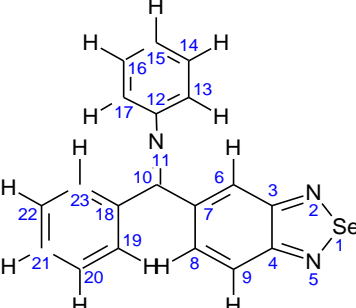
Table 1. UV-visible (λ max nm) spectral data, yield, melting points, and Rf value of selected compounds.

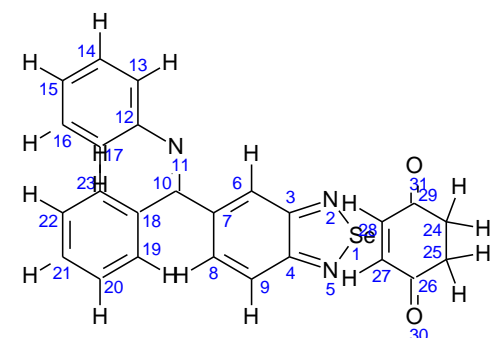
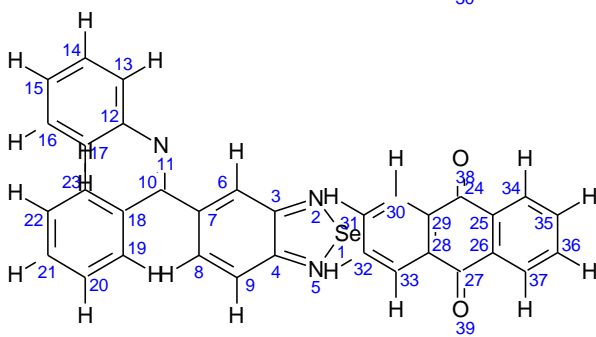
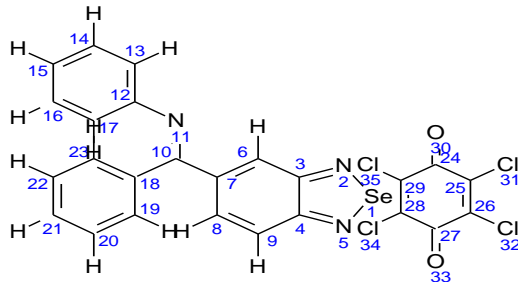
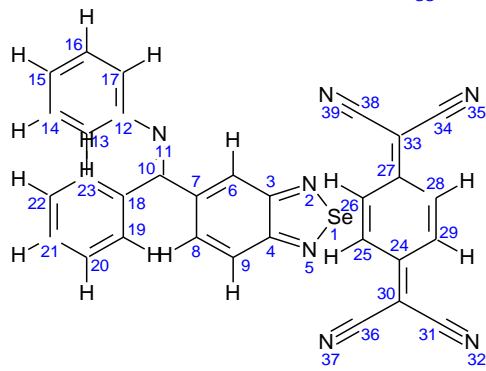
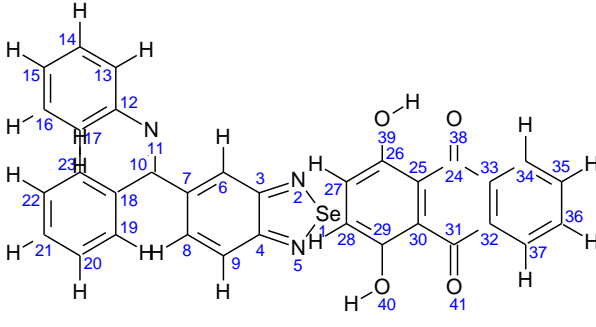
Seq.	Compound	λ max of n- π^* and π - π^* transitions	yield of compound	melting point	Rf value
1	I	(225, 273, 355) nm	80%	95 °C.	0.78
2	II	(220, 233, 240, 243, 250, 270, 345) nm	76%	(105–110) C°.	0.93
3	III	(205, 230, 236, 270, 280, 355) nm	76%	107 C°	0.92
4	IV	(215, 230, 240, 248, 252, 275, 350) nm	64%	(118–208) C°	0.85
5	V	(215, 237, 240, 248, 285, 350) nm	71%	(170–230) C°	0.88
6	VI	(210, 220, 225, 245, 250, 365, 400) nm	71%	(149–260) C°	0.92
7	VII	(210, 225, 230, 245, 255, 273, 335, 473) nm	70%	(167–187) C°.	0.88

Table 2. The spectral FT-IR data of synthesized compounds.

functional group	Compounds						
	I	II	III	IV	V	VI	VII
Ar. C–H (cm ⁻¹)	3061	3063	3063	3070	3063	3051	3061
Ar. (C=O) (cm ⁻¹)	1649	-	1724 -1788	1737-1795	1768	-	1691
Ar. C=N(cm ⁻¹)	1579-1600	1593-1637	1597-1639	1639-1676	1639-1683	1651-1676	1629
Ar. C=C(cm ⁻¹)	1490-1500	1448-1556	1504-1575	1545-1589	1570-1591	1541	1539-1589
Aliphatic C=C(cm ⁻¹)	-	-	-	-	-	1433	-
Ar. C-Se-N(cm ⁻¹)	3248.54	3250	3259	3319	3356	31380	3210
Aliphatic C≡N(cm ⁻¹)	-	-	-	-	-	2222	-
Ar. OH (cm ⁻¹)	-	-	-	-	-	-	3500-3600
Ar. C-Cl(cm ⁻¹)	-	-	-	-	550-880	-	-
Ar. C-N(cm ⁻¹)	-	1325	1325	1330	1325	3354	1357

Table 3. The spectral¹H-NMR data of synthesized compounds.

Seq	compounds	synthesized compounds Structure	Signals of ¹ H-NMR TMS= 0 ppm (DMSO-d ₆)
1	I		δ Ar. ₁₄ C-H, ₁₆ C-H (2H, m, δ 7.52); Ar. ₁₅ C-H, ₁₇ C-H (2H, m, δ 7.74); Ar. ₁₃ C-H, (1H, t, δ 7.89); Ar. ₉ C-H, (1H, d, δ 7.90); Ar. ₈ C-H, (1H, d, δ 8.02); Ar. ₆ C-H, (1H, s, δ 8.11).
	II		δ Ar. ₁₃ C-H, ₁₄ C-H, ₁₅ C-H, ₁₆ C-H, ₁₇ C-H, ₂₀ C-H, ₂₁ C-H, ₂₂ C-H (8H, m, δ 7.5-7.7); Ar. ₁₉ C-H, ₂₃ C-H (2H, m, δ 8.2); Ar. ₉ C-H, (1H, d, δ 8.01); Ar. ₈ C-H, (1H, d, δ 8.03); Ar. ₆ C-H, (1H, s, δ 8.10)

2	III		<p>δ Ar. $_{13}\text{C-H}$, $_{14}\text{C-H}$ (2H, m, δ 7.53), δ Ar. $_{15}\text{C-H}$, $_{16}\text{C-H}$ (2H, m, δ 7.58), δ Ar. $_{17}\text{C-H}$, $_{19}\text{C-H}$, $_{20}\text{C-H}$, $_{21}\text{C-H}$, $_{22}\text{C-H}$, (5H, m, δ 7.53 -7.77), δ Ar. $_{25}\text{C-H}$, $_{26}\text{C-H}$, $_{28}\text{C-H}$, $_{29}\text{C-H}$ (4H, m, δ 7.85 -7.90) Ar. $_{23}\text{C-H}$ (1H, d, δ 7.52); Ar. $_{9}\text{C-H}$, (1H, d, δ 8.01); Ar. $_{8}\text{C-H}$, (1H, d, δ 8.02); Ar. $_{6}\text{C-H}$, (1H, s, δ 8.10)</p>
3	IV		<p>δ Ar. $_{13}\text{C-H}$, $_{15}\text{C-H}$ (2H, m, δ 7.58-7.69), δ Ar. $_{14}\text{C-H}$, $_{16}\text{C-H}$, $_{17}\text{C-H}$, (3H, m, δ 7.57-7.63), δ Ar. $_{20}\text{C-H}$, $_{21}\text{C-H}$, $_{19}\text{C-H}$, $_{22}\text{C-H}$, (4H, m, δ 7.57 -7.76), δ Ar. $_{30}\text{C-H}$, $_{31}\text{C-H}$, $_{32}\text{C-H}$, $_{33}\text{C-H}$, $_{34}\text{C-H}$, $_{35}\text{C-H}$, $_{36}\text{C-H}$, $_{37}\text{C-H}$ (8H, m, δ 7.85 -7.95) Ar. $_{23}\text{C-H}$ (1H, d, δ 8.3); Ar. $_{9}\text{C-H}$, (1H, d, δ 8.26); Ar. $_{8}\text{C-H}$, (1H, d, δ 8.20); Ar. $_{6}\text{C-H}$, (1H, s, δ 8.09)</p>
4	V		<p>δ Ar. $_{13}\text{C-H}$ (1H, d, δ 8.03), δ Ar. $_{14}\text{C-H}$, $_{15}\text{C-H}$, $_{16}\text{C-H}$ (3H, m, δ 7.86-7.87), δ Ar. $_{17}\text{C-H}$, $_{20}\text{C-H}$, $_{21}\text{C-H}$ (3H, m, δ 7.58-7.77), δ Ar. $_{23}\text{C-H}$ (1H, d, δ 7.62); Ar. $_{19}\text{C-H}$, (1H, d, δ 7.9), $_{22}\text{C-H}$ (1H, t, δ 7.59); Ar. $_{9}\text{C-H}$, (1H, d, δ 8.02); Ar. $_{8}\text{C-H}$, (1H, d, δ 8.01); Ar. $_{6}\text{C-H}$, (1H, s, δ 8.10);</p>
5	VI		<p>δ Ar. $_{13}\text{C-H}$, (1H, d, δ 8.01) δ Ar. $_{23}\text{C-H}$, $_{14}\text{C-H}$ (2H, m, δ 7.86-7.88), δ Ar. $_{15}\text{C-H}$, $_{16}\text{C-H}$ (2H, m, δ 7.72-7.76), δ Ar. $_{17}\text{C-H}$, $_{20}\text{C-H}$, $_{21}\text{C-H}$, (3H, m, δ 7.86 -7.88), δ Ar. $_{25}\text{C-H}$, $_{26}\text{C-H}$, $_{28}\text{C-H}$, $_{29}\text{C-H}$ (4H, m, δ 7.88 -7.89), Ar. $_{22}\text{C-H}$, $_{19}\text{C-H}$, (2H, t, δ 7.60-7.63); Ar. $_{9}\text{C-H}$, (1H, d, δ 8.01); Ar. $_{8}\text{C-H}$, (1H, d, δ 8.02); Ar. $_{6}\text{C-H}$, (1H, s, δ 8.09);</p>
6	VII		<p>δ Ar. $_{13}\text{C-H}$, $_{14}\text{C-H}$ (2H, m, δ 7.49-8.02), δ Ar. $_{15}\text{C-H}$, $_{16}\text{C-H}$ (2H, t, δ 8.02-8.03), Ar. $_{17}\text{C-H}$ (1H, s, δ 8.31), δ Ar. $_{21}\text{C-H}$, $_{22}\text{C-H}$ (2H, t, δ 7.49-8.02), $_{19}\text{C-H}$, $_{23}\text{C-H}$, (2H, d, δ 7.57 -7.76), δ Ar. $_{27}\text{C-H}$, $_{28}\text{C-H}$, $_{34}\text{C-H}$, $_{35}\text{C-H}$, $_{36}\text{C-H}$, $_{37}\text{C-H}$ (6H, m, δ 8.30 -8.03) Ar. $_{20}\text{C-H}$ (1H, d, δ 8.03); Ar. $_{9}\text{C-H}$, (1H, d, δ 8.31); Ar. $_{8}\text{C-H}$, (1H, d, δ 8.30); Ar. $_{6}\text{C-H}$, (1H, s, δ 8.32) δ Ar. $_{39}\text{O-H}$, $_{40}\text{O-H}$ (2H, s, δ 12.7)</p>

Results and Discussion:

The current research included the synthesis of charge transfer complexes that were produced by N-phenyl 3,4-selenadiazobenzophenone imine²³ (prepared in the second step) by reacting N-phenyl 3,4-selenadiazobenzophenone imine²³ using

acetonitrile as solvent and adding five types of different quinones (each quinone has a separate reaction) to obtain new charge transfer complexes compounds (III–VII). The transitions of n- π^* typically experienced a significant shift in blue during synthesis complexes of charge-transfer. The

selenium atom is responsible for the deviating of the electron cloud around it and for a change in the evolution of the charge-transfer complexes. The bands of absorption shifted to shorter wave lengths when quinones' electron donors decreased the π - π^*

and n - π^* transitions, chromophore group conjugate effects, increasing the required energy for transitions of π - π^* and n - π^* . Are provided in Figs. 1-7, as shown in Table1.

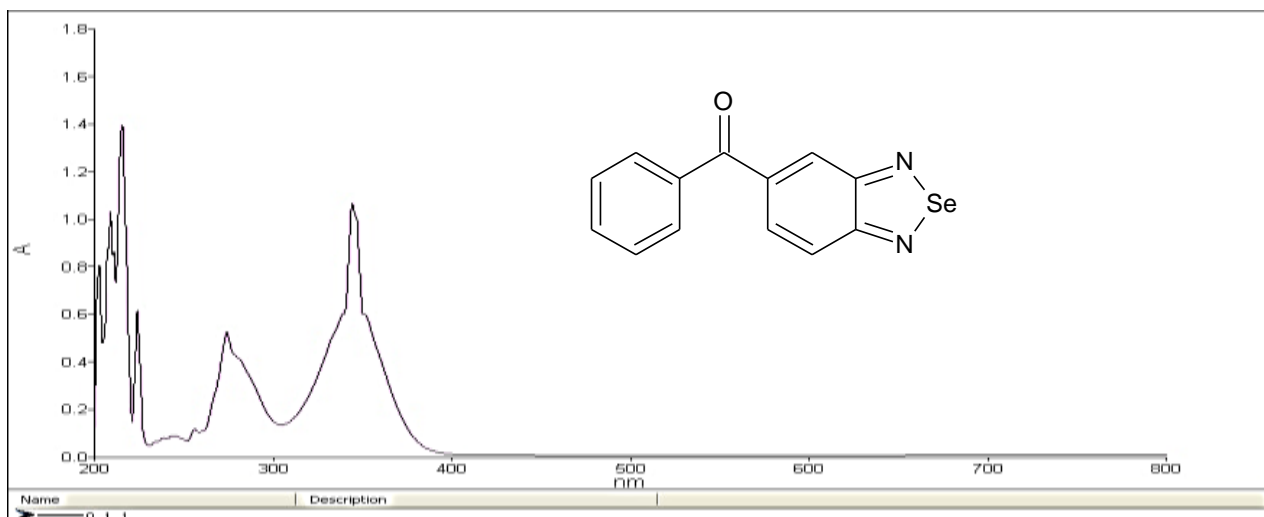


Figure 1. UV-Visible spectrum of compound (I).

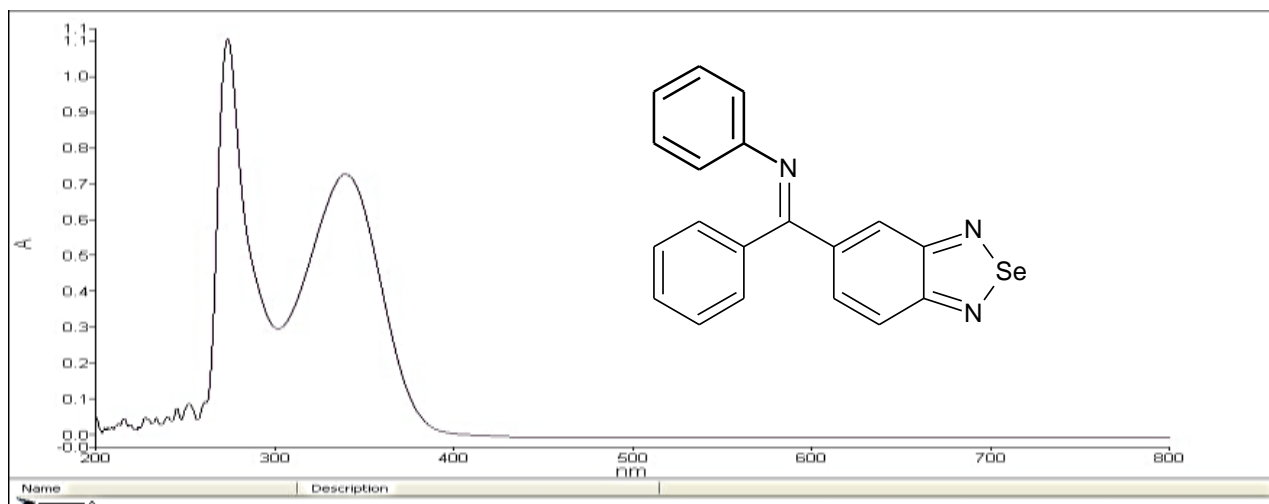


Figure 2. UV-Visible spectrum of compound (II).

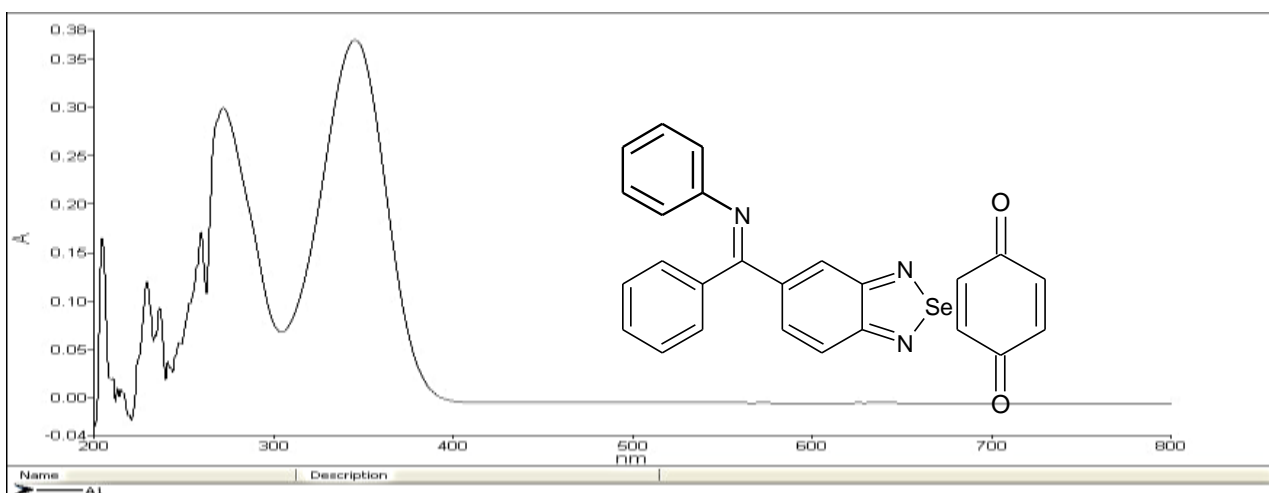


Figure 3. UV-Visible spectrum of compound (III).

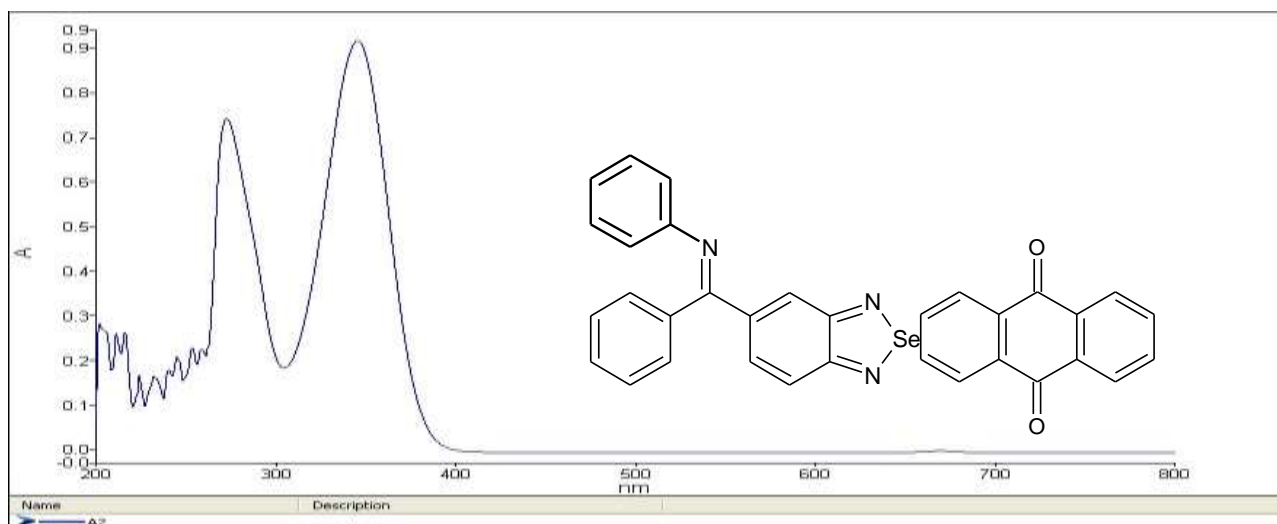


Figure 4. UV-Visible spectrum of compound (IV).

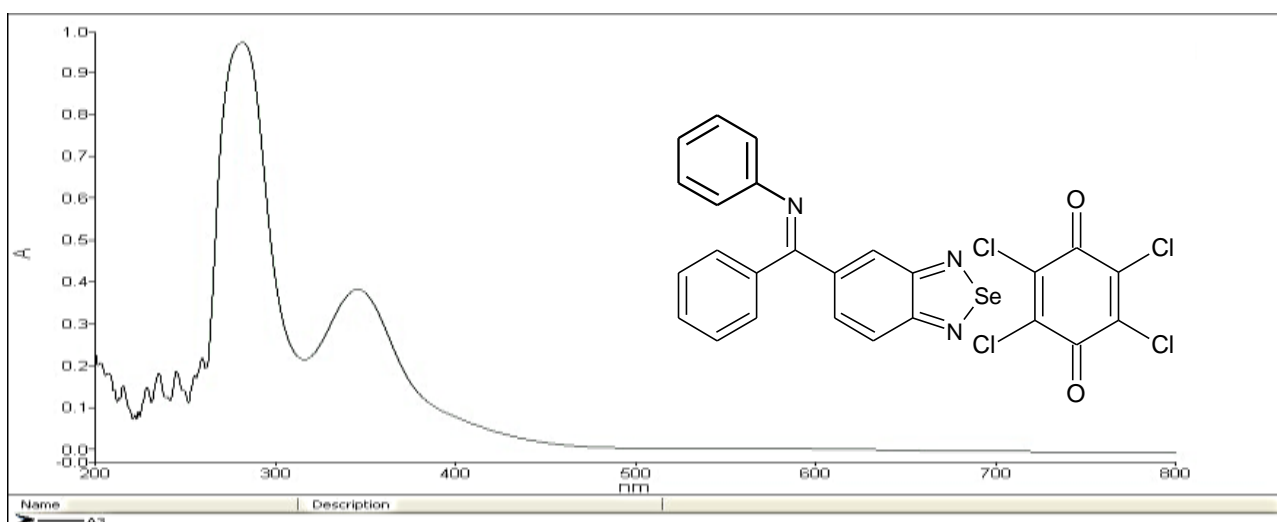


Figure 5. UV-Visible spectrum of compound (V).

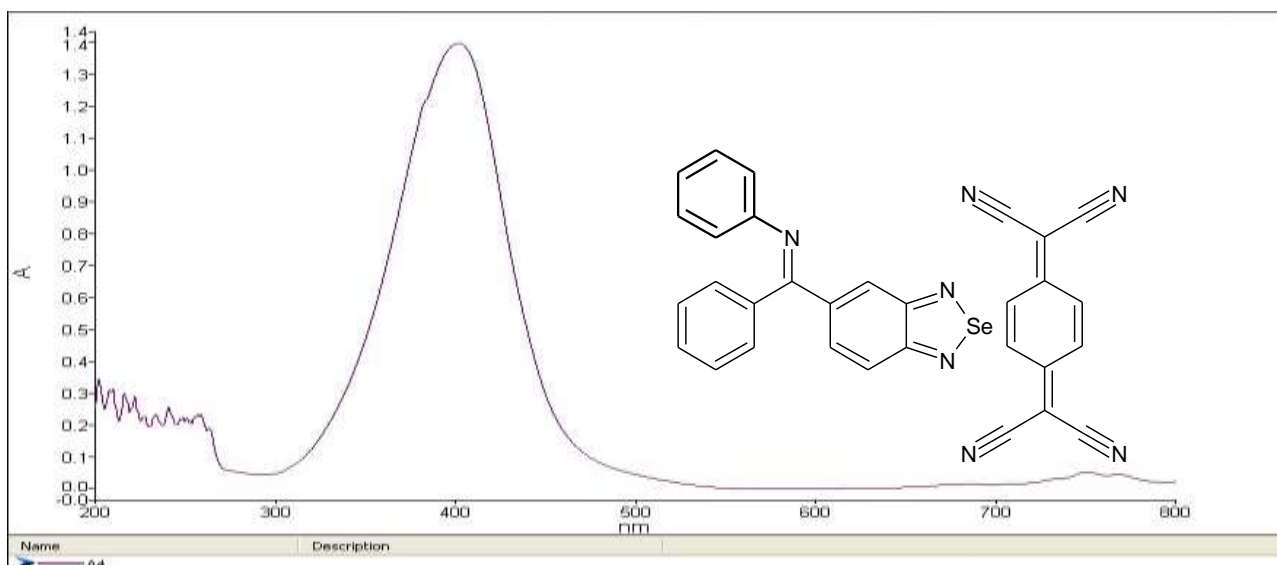


Figure 6. UV-Visible spectrum of compound (VI).

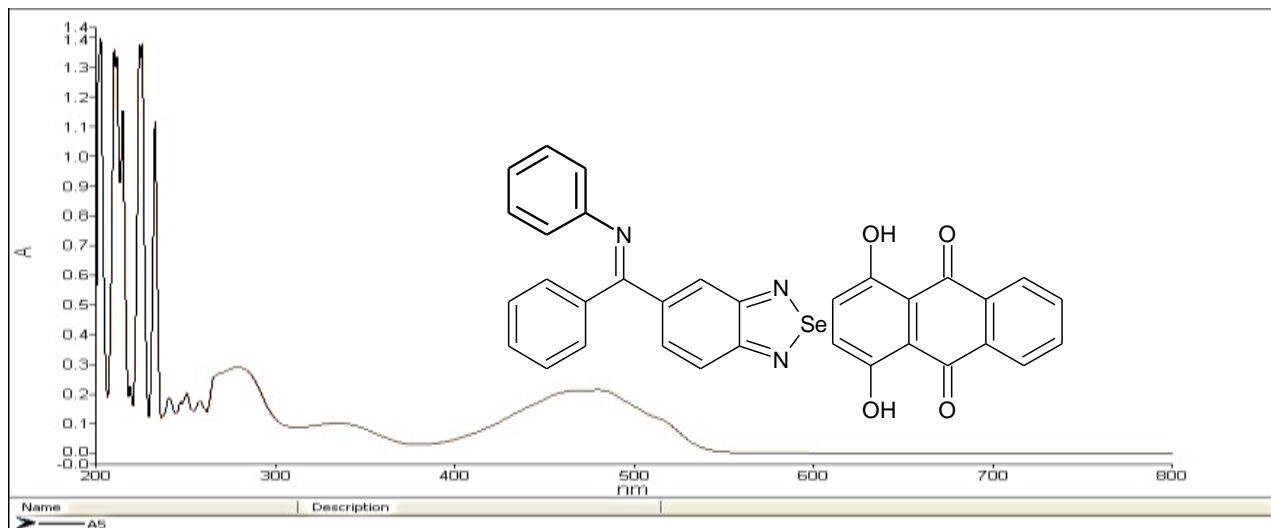


Figure 7. UV-Visible spectrum of compound (VII).

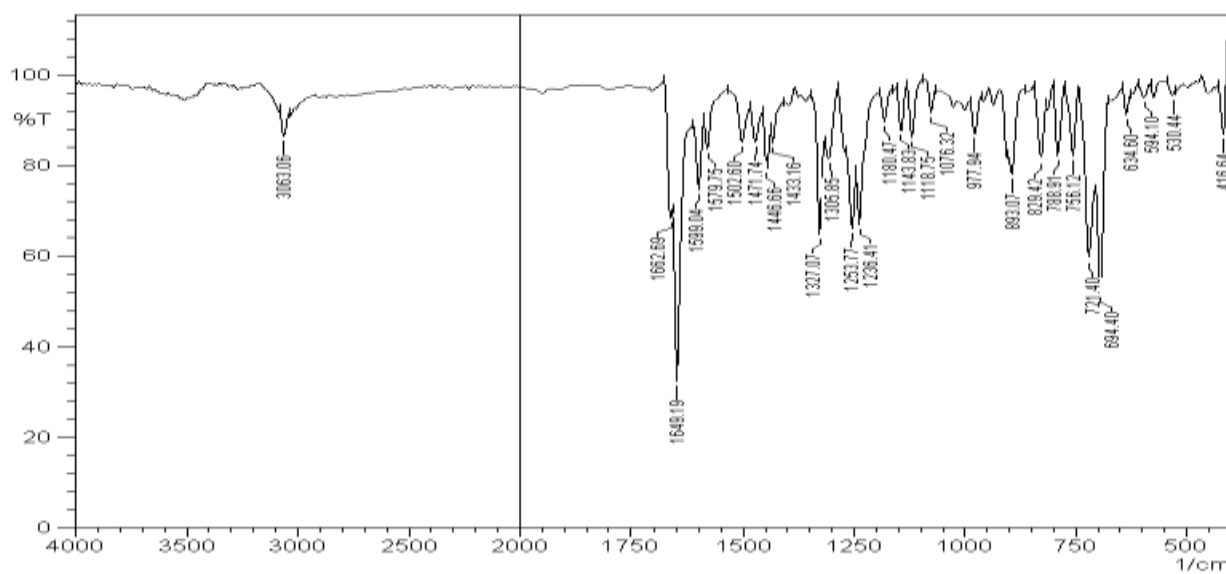


Figure 8. FT-IR spectrum of compound (I).

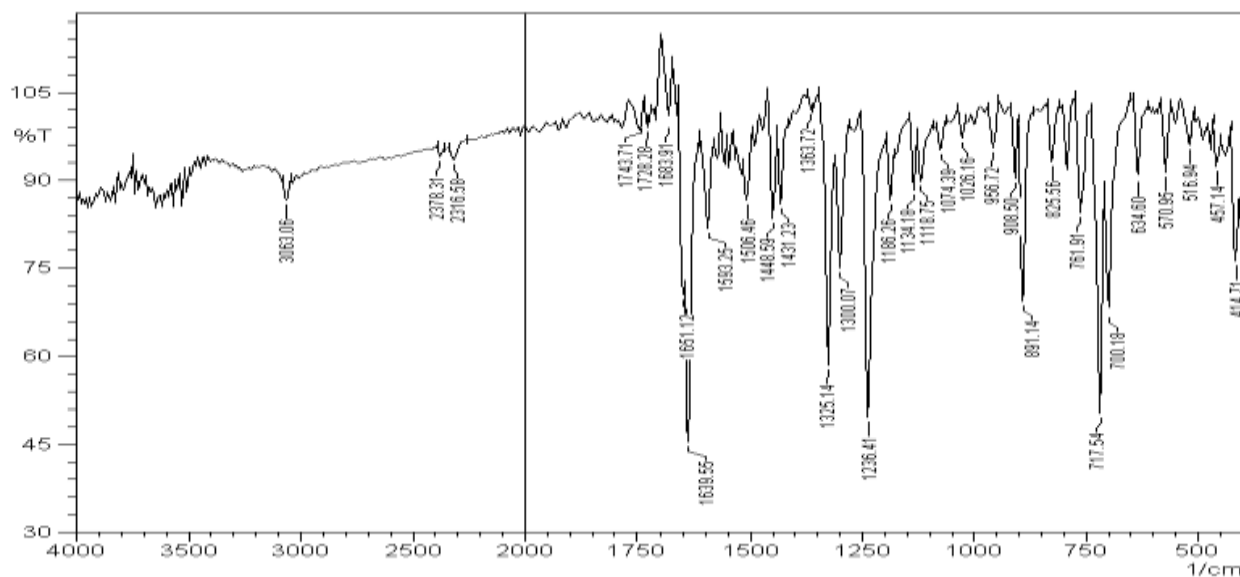


Figure 9. FT-IR spectrum of compound (II).

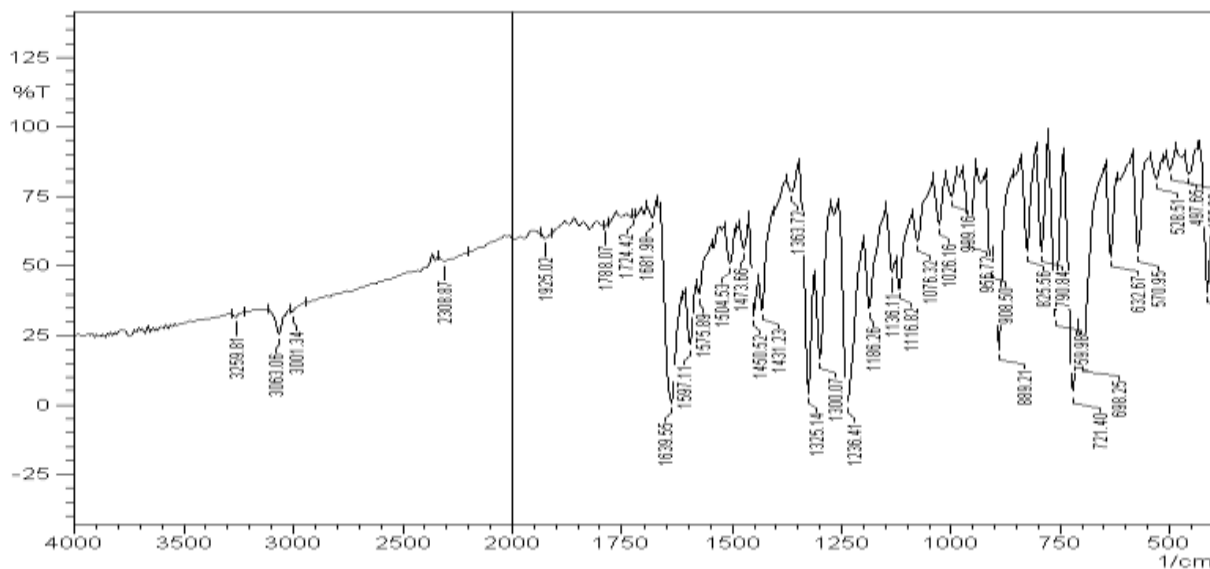


Figure 10. FT-IR spectrum of compound (III).

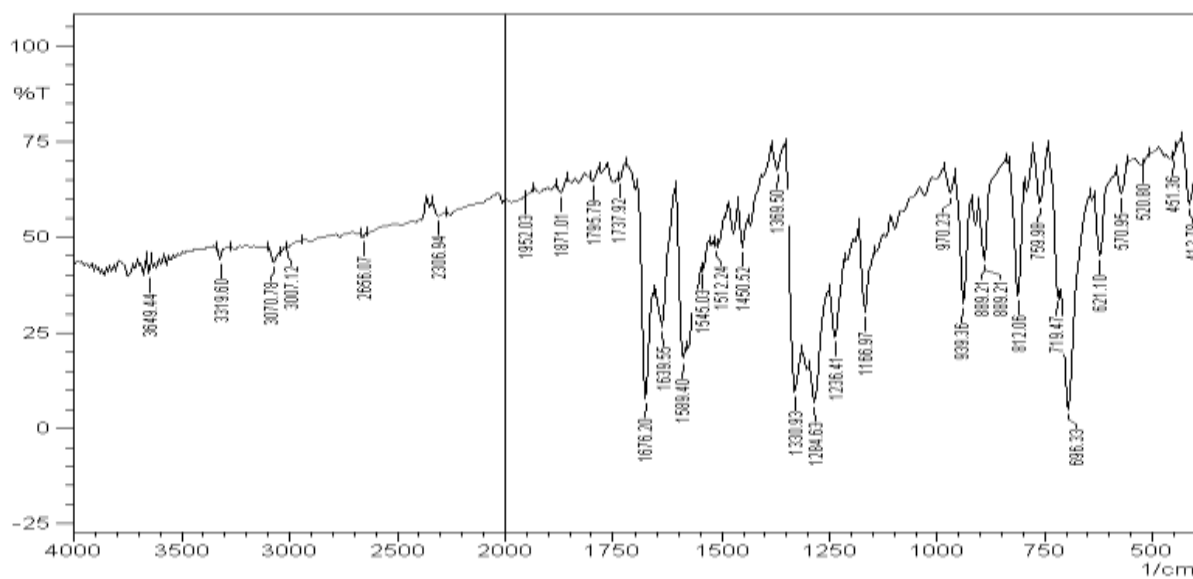


Figure 11. FT-IR spectrum of compound (IV).

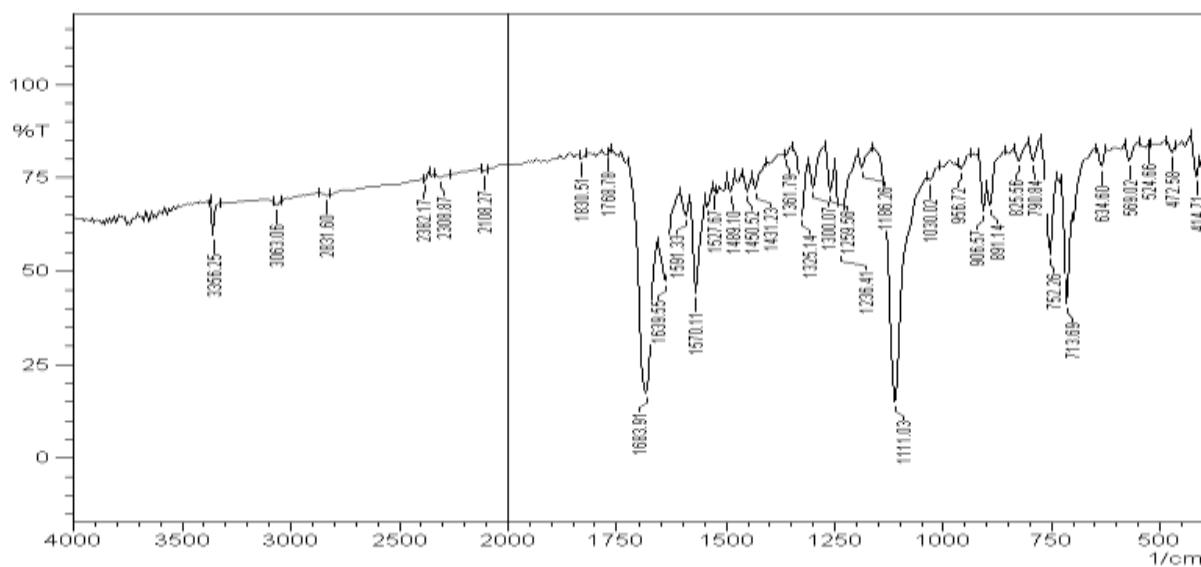


Figure 12. FT-IR spectrum of compound (V).

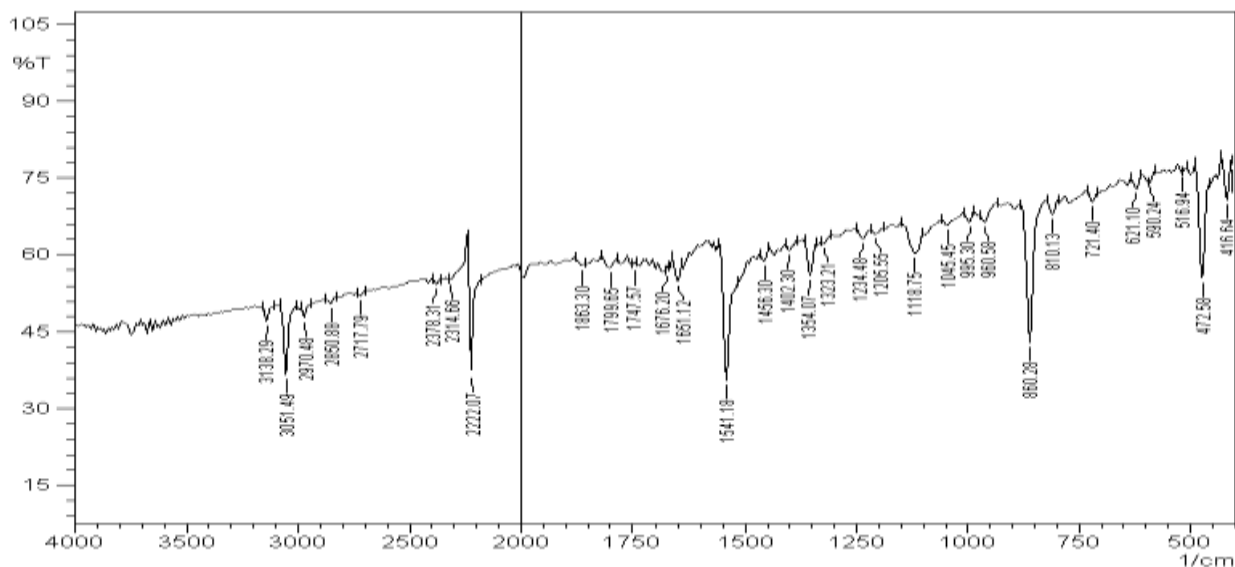


Figure 13. FT-IR spectrum of compound (VI).

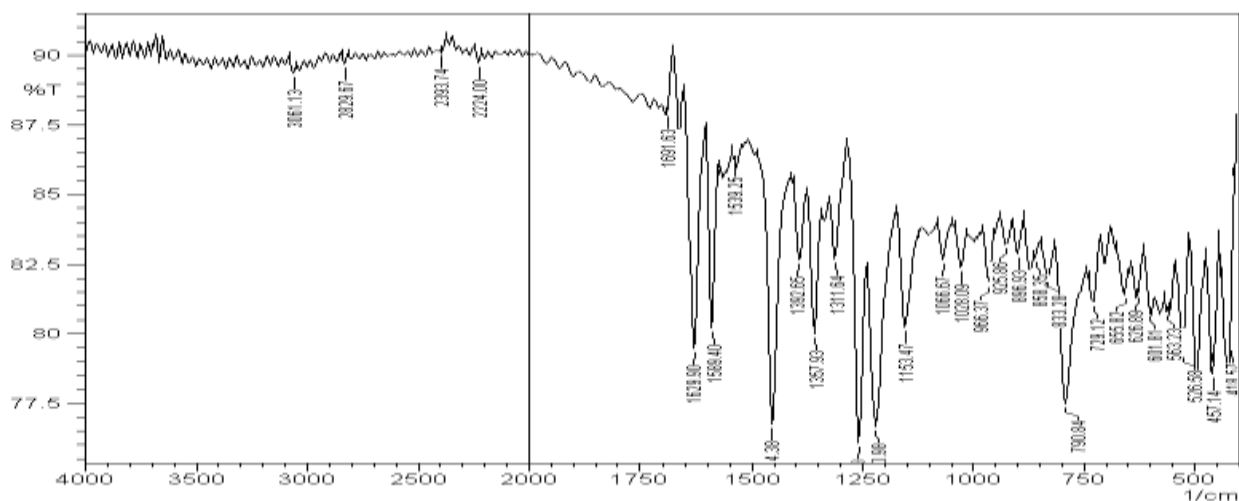


Figure 14. FT-IR spectrum of compound (VII).

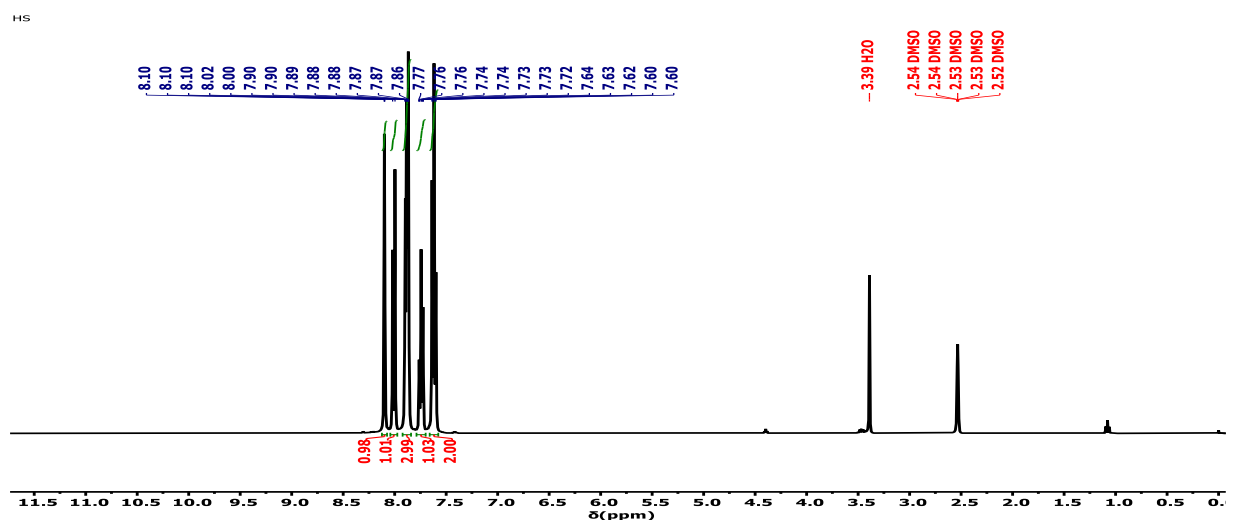


Figure 15. ¹H-NMR spectrum of compound 3,4-Selenadiazobenzophenone (I).

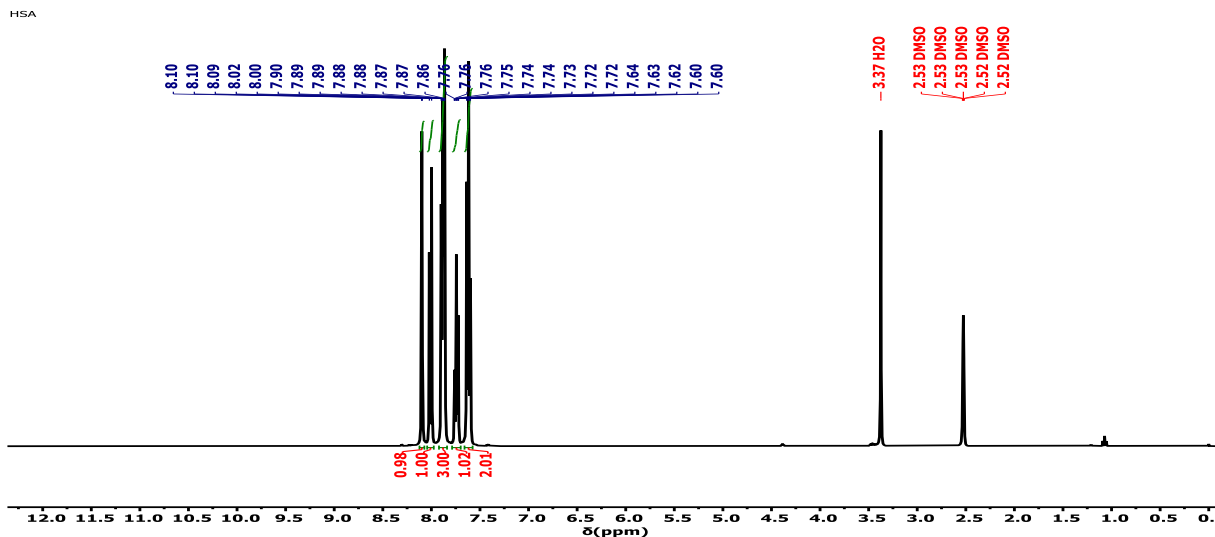


Figure 16. ¹H-NMR spectrum of compound (II).

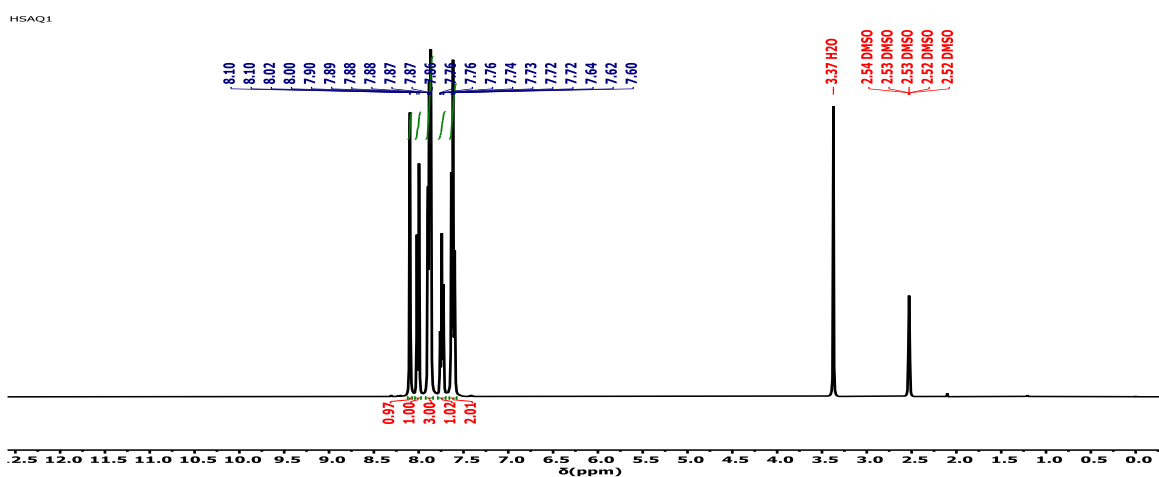


Figure 17. ¹H-NMR spectrum of compound (III).

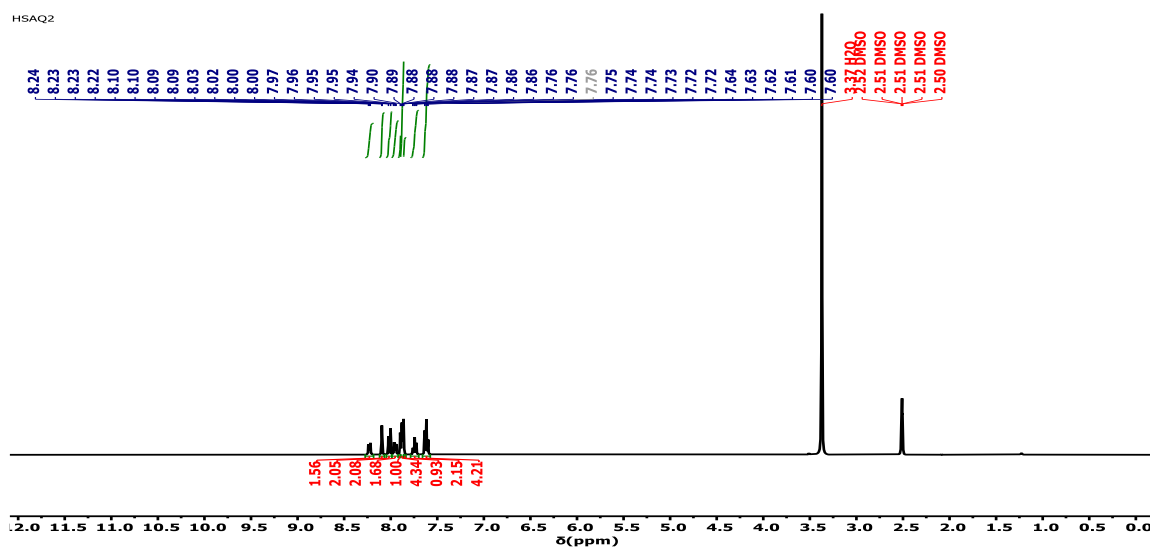


Figure 18. ¹H-NMR spectrum of compound (IV).

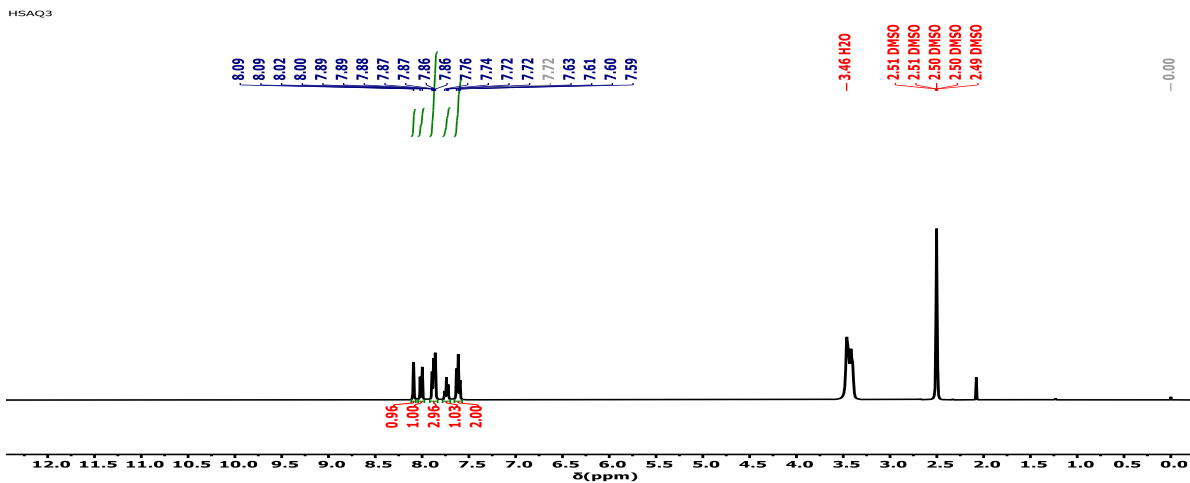


Figure 19. ¹H-NMR spectrum of compound (V).

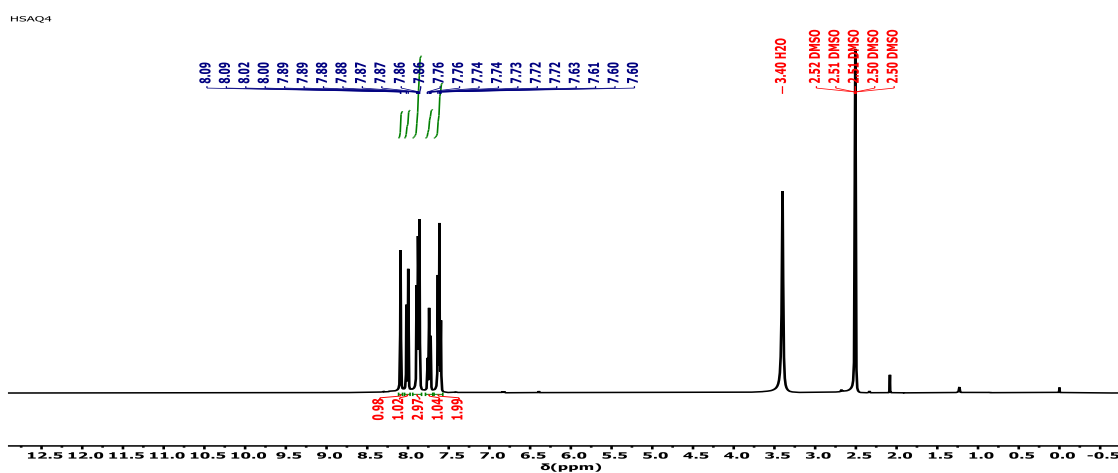


Figure 20. ¹H-NMR spectrum of compound (VI).

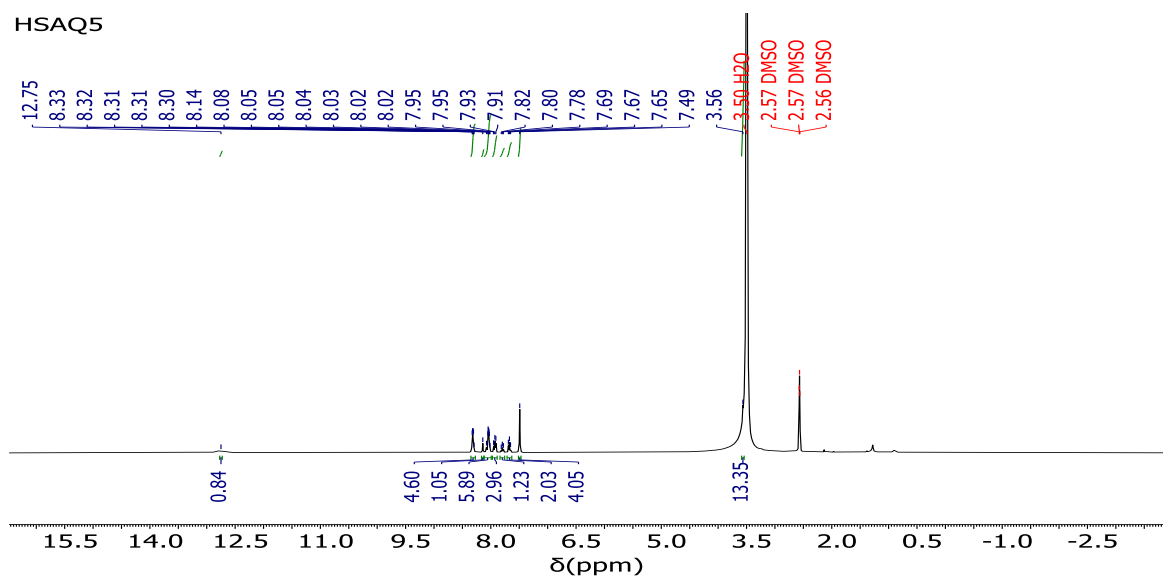


Figure 21. ¹H-NMR spectrum of compound (VII).

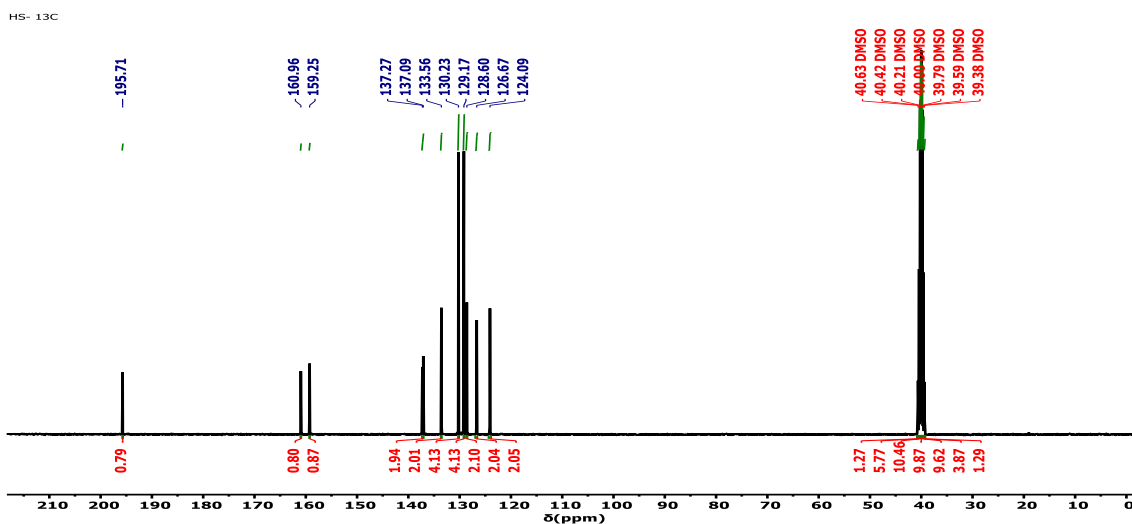


Figure 22. ^{13}C NMR spectrum of compound 3,4-Selenadiazobenzophenone.

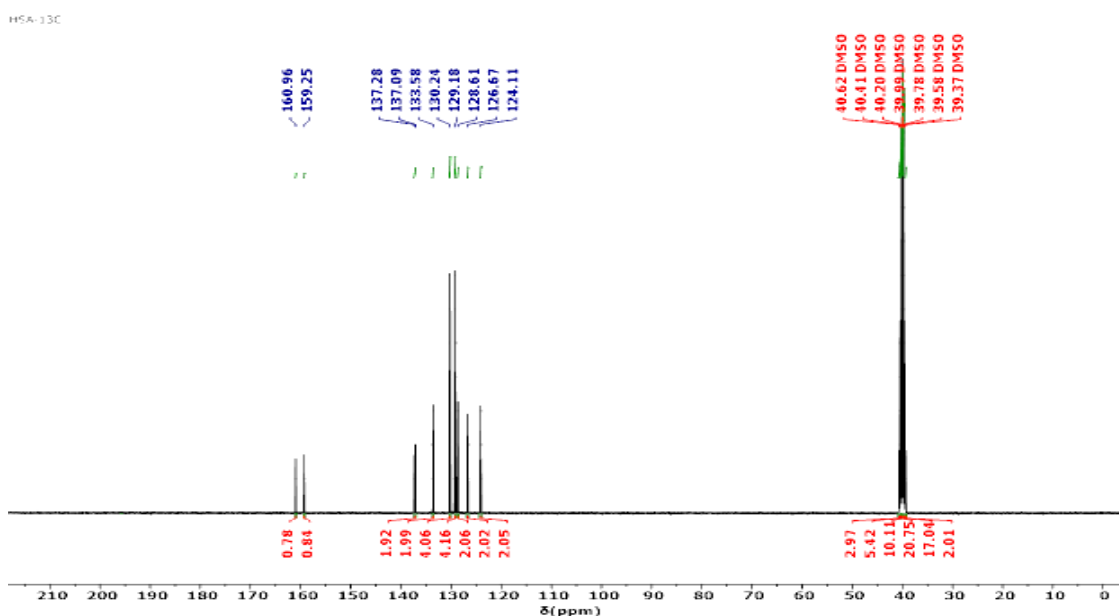
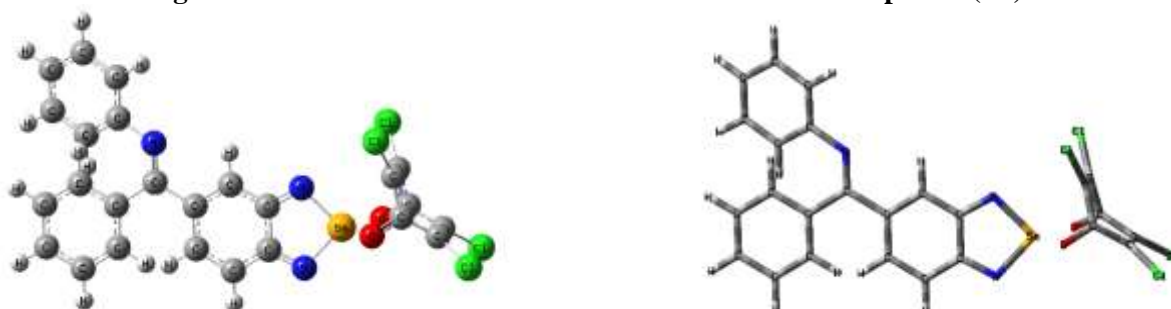
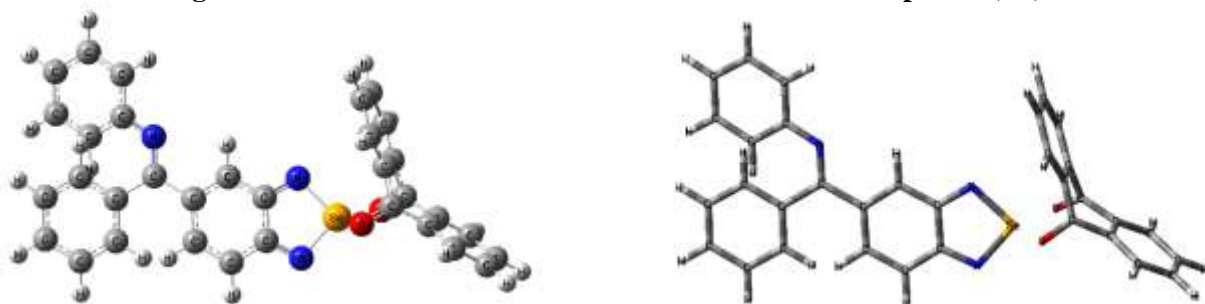
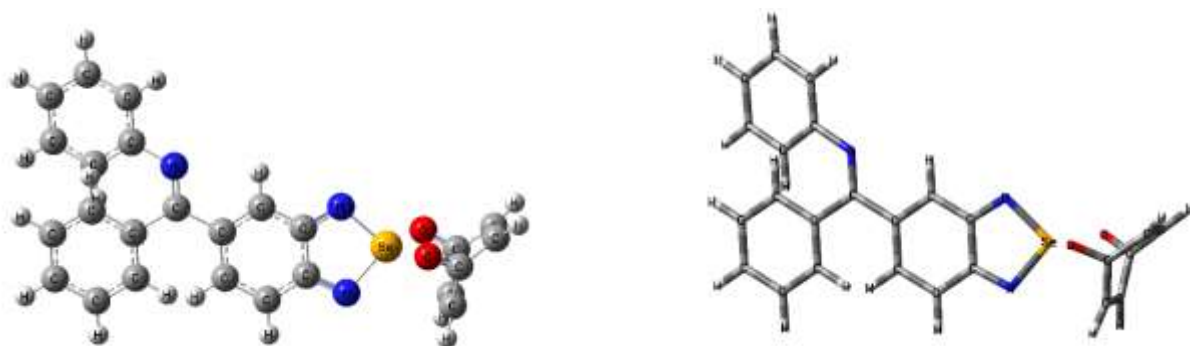
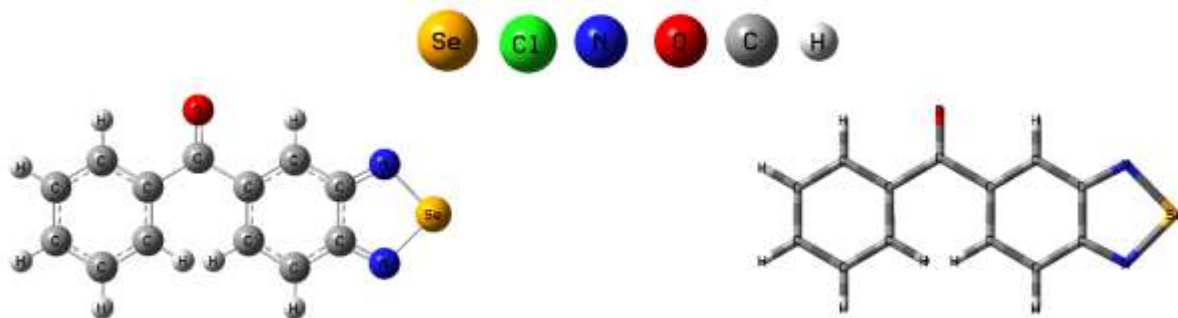


Figure 23. ^{13}C NMR spectrum of compound N-phenyl 3,4-selenadiazobenzophenone imine.

UV-visible spectra were recorded at 200-750 nm in (DMSO) solvent, $n-\pi^*$ and $\pi-\pi^*$ are two different types of electronic transitions²⁴, are provided, such as Figs 1–7, as shown in Table 1. λ_{max} for prepared complex compounds with a wavelength range of 205–473 nm. The infrared (IR) spectra of all synthesized complexes showed common characteristic bands and specific regions or other locations. The synthesized compounds suggested structures were verified by using the IR spectrum^{25,26}. They are provided in Figs. 8–14 and Table 2. Ar. C-H appeared at 3051-3070 cm^{-1} for N-

phenyl 3,4-selenadiazobenzophenone imine and charge transfer complexes derivatives, while Ar. (C=O) appeared at 1649-1795 cm^{-1} , Ar. C=N at 1579-1683 cm^{-1} , whereas aliphatic C \equiv N at 2222 cm^{-1} , Ar. C=C at 1448-1591 cm^{-1} , Aliphatic C=C at 1433 cm^{-1} , Ar. C-Se-N at 3138-3356 cm^{-1} , Ar. O-H at 3500-3600 cm^{-1} , and Ar. C-I at 550-800 cm^{-1} . ^1H -NMR spectra of the compounds (I–VII) showed all the peaks as expected with explanations. Figs 15–21 and Table 3 show DMSO spectra for each selected compound.



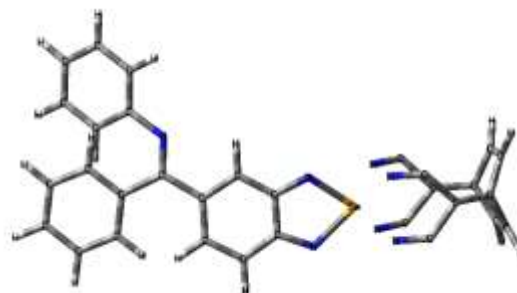
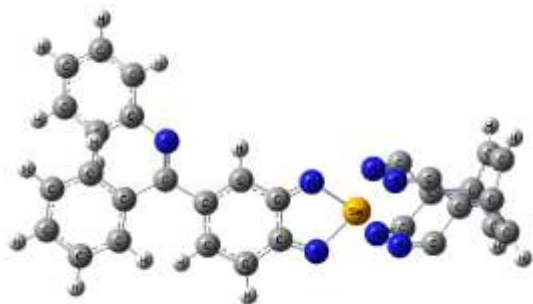


Figure 29. Molecular structure Ball and tube model of compound (VI).

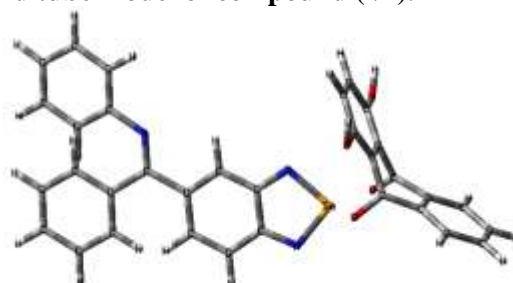


Figure 30. Molecular structure Ball and tube model of compound (VII).

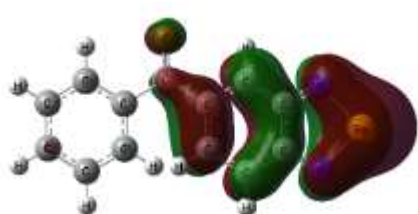


Figure 31. Mo. orbital (HOMO) of compound (I). Figure 32. Mo. orbital (LUMO) of compound (I).

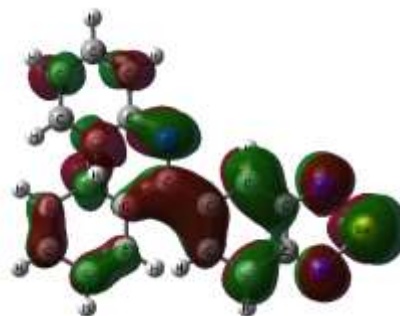
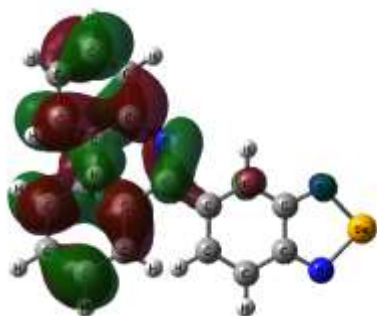


Figure 33. Mo. orbital (HOMO) of compound (II). Figure 34. Mo. orbital (LUMO) of compound (II).

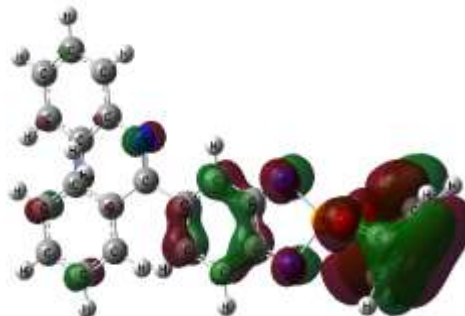
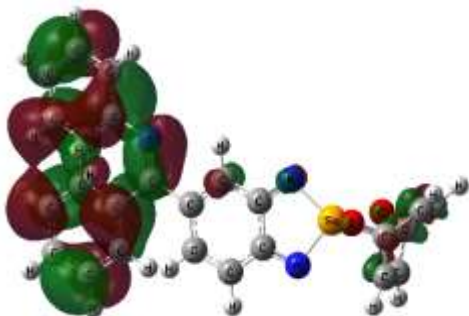


Figure 35. Mo. orbital (HOMO) of compound (III). Figure 36. Mo. orbital (LUMO) of compound (III).

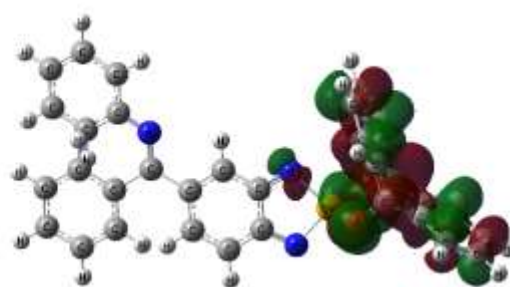
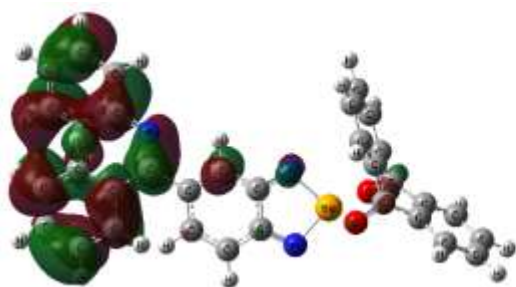


Figure 36. Mo. orbital (HOMO) of compound (IV). Figure 37. Mo. orbital (LUMO) of compound (IV).

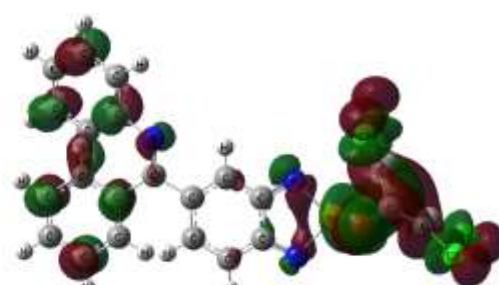
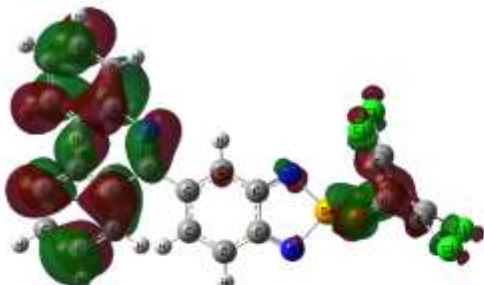


Figure 38. Mo. orbital (HOMO) of compound (V). Figure 39. Mo. orbital (LUMO) of compound (V).

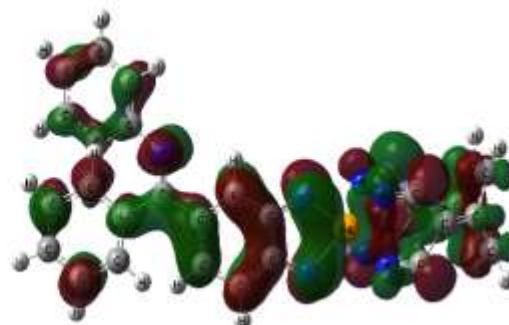
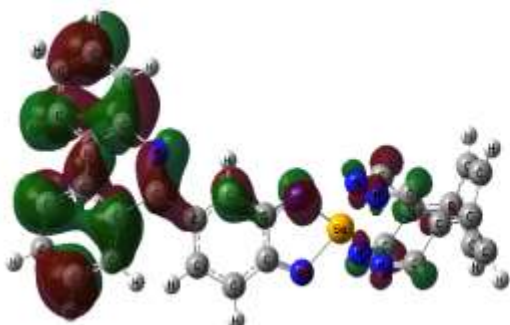


Figure 40. Mo. orbital (HOMO) of compound (VI). Figure 41. Mo. orbital (LUMO) of compound (VI).

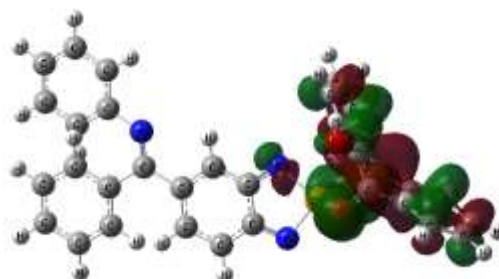
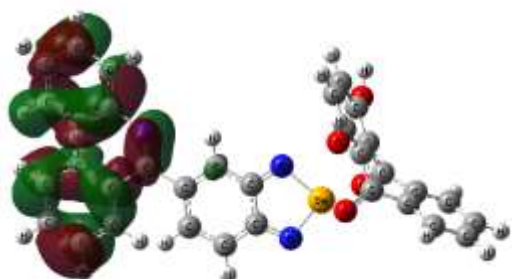


Figure 42. Mo. orbital (HOMO) of compound (VII). Figure 43. Mo. orbital (LUMO) of compound (VII).

Computational Analysis

The charge-transfer complex compounds of N-phenyl 3,4-selenadiazo benzophenone imine under analysis were labeled as shown in Figs.24- 43. It was determined how well the method described the compound's properties in the gas phase. The functional theory of density (DFT) at hybrid functional (B3LYP), the levels of functional computational its combine between Parr's, and Lee, Yang correlation with exchange Becke's, was used to analyze the electronic characteristics and geometric structures of these compounds by all quantum calculations^{27,28}. Using the basis of the set of 3–21G and the Gaussian (G09W) software, this method

described each atom²⁹. Using estimated DFT-based descriptors, the compounds' reactivity and stability were assessed³⁰⁻³³through the mathematical relations as in the Eq.1, Eq.2, Eq.3 and Eq.4.

$$\begin{aligned} \mu &= \left(\frac{\delta E}{\delta N} \right)_{V(\vec{r}),T} \dots \dots 1 \\ \eta &= \frac{1}{2} \left(\frac{\delta^2 E}{\delta N^2} \right)_{V(\vec{r}),T} \dots \dots 2 \\ S &= \frac{1}{2\eta} \dots \dots 3 \\ \omega &= \frac{\mu^2}{2\eta} \dots \dots 4 \end{aligned}$$

Where the μ = (chemical potential), η = (chemical hardness), S = (chemical softness), and ω = (electrophilicity), while E = (the total electron energy), N = (number of electrons), and $V(r \rightarrow)$ is (the external potential) respectively. The above global quantities were calculated by using two variations approaches; the first is a difference in a finite approximation, this is based on the changes in total electronic energy that occurs after the neutral molecule whenever an electron is added or removed. The energies of (HOMO) and (LUMO) different for molecules serve as the foundation for Koopman's theory^{30,33,34}. Global quantities that are derivable from Eqs. 5 and 6 are approximated using finite differences.

$$\chi = \frac{(IP + EA)}{2} \dots 5$$

$$\eta = \frac{(IP - EA)}{2} \dots 6$$

But Koopman's theory, given by Eq.7, Eq.8.

$$\chi = \frac{(E_{HOMO} + E_{LUMO})}{2} \dots 7$$

$$\eta = \frac{(E_{HOMO} - E_{LUMO})}{2} \dots 8$$

The equilibrium geometries for all CT (charge-transfer) complex compounds in the gaseous phase were carefully tuned at level of the (DFT)³² for theory using the functional of a (B3LYP) in (G09W) and the basis standard established (3-21G) (see Figs. 24- 43). The energies of (HOMO) Molecular Orbital High Occupied and (LUMO) Molecular Orbital Low Unoccupied are the states of electrons, defining certain regions where atomic and molecular orbitals combine linearly, leading to the existence of electrons with quantized energy. The relationship between the energy band gap (Eg) Eq.9, Eq.6. and the difference in (LUMO) and (HOMO)³⁵. The property of the Eg is essential in solids because it makes material prediction possible, if it is an insulator, semiconductor, or conductor. It depicts the difference in energy between the higher full energy level and the lower level of virtual energy.³⁶ See Figs. (24- 43) and Table4.

$$Eg = E_{LUMO} - E_{HOMO} \dots 9$$

Electronegativity and Electrophilicity

The molecule's ability to take up electrons is measured by chemical electrophilicity, which is determined by chemical electrophilicity, which is dependent on chemical hardness and chemical potential, where hardness is resistance to deformation and change. On the other hand, electronegativity measures an atom's capacity to attract an electron density (a shared pair of electrons) towards itself. Calculating electrophilicity and electronegativity can be done using relationships in Eq.10, Eq.11.^{22,30,31}; see Table 5.

$$\chi = \frac{(E_{HOMO} + E_{LUMO})}{2} \dots 10$$

$$\omega = \frac{\chi^2}{2\eta} \dots 11$$

Ionization Potential, and Electron Affinity

Measurement of the bond's strength is done via the ionization potential among an atom and an electron. It possesses the same amount of energy as what is needed to expel one electron from a neutral atom in the gas phase. When an atom takes an electron, energy is released, which is referred to as having a "electron affinity." It is the necessary energy to remove an electron from a negatively charged ion. This is consistent with Koopman's theory²⁸, as seen in Eq.12, Eq.13 and Table 6.

$$I.P = -E_{HOMO} \dots 12$$

$$E.A = -E_{LUMO} \dots 13$$

HSAB Principle (Acid Base Hardness Softness)

When utilized as acids and bases in chemistry, this principle describes how atoms or molecules behave. First, it must be shown that soft and hard acids are acceptors, whereas hard and soft bases are donors. Eq.14, Eq.15. are used to show both hardness and softness³⁷⁻³⁹.

$$\eta = \frac{(IP - EA)}{2} \dots 14$$

$$\delta = \frac{1}{2\eta} \dots 15$$

Chemical softness and hardness are indicated, respectively, by the symbols (σ) and (η). based on Table 6.

Table 4. The electronic state compounds for charge-transfer complexes.

Compound,	HOMO, (eV)	LUMO, (eV)	Eg, (eV)
I	-6.43	-2.8848	3.545191
II	-3.35608	-3.01868	0.337404
III	-4.891	-2.7629	2.128094
IV	-3.06466	-2.56781	0.496855
V	-3.8894	-3.60152	0.287882
VI	-3.77403	-3.30357	0.470461
VII	-3.36479	-2.57842	0.786369

Table 5. Electronegativity and electrophilicity of compounds for the charge-transfer complex.

Compound	Electronegativity (eV) (X)	Electrophilicity (eV) (w)
I	-4.6574	-6.11853
II	-3.18738	-30.1105
III	-3.82695	-6.882
IV	-2.81624	-15.9628
V	-3.74546	-48.7299
VI	-3.5388	-26.6188
VII	-2.9716	-11.2294

Table 6. Ionization potential, electron affinity, softness, and hardness for charge-transfer complex compounds.

Compound	Ionization potential (eV) (I.P)	Electron affinity (eV) (E.A)	Softness (δ)	Hardness (η)
I	6.4299951	2.8848042	-1.7726	-0.28207
II	3.3560814	3.0186774	-0.1687	-2.96381
III	4.8909975	2.7629034	-1.06405	-0.4699
IV	3.0646623	2.5678077	-0.24843	-2.01266
V	3.8893974	3.6015156	-0.14394	-3.47365
VI	3.774027	3.3035661	-0.23523	-2.12558
VII	3.3647886	2.5784196	-0.39318	-1.27167

Conclusion:

The current work outlines simple and doable procedures for creating a variety of unique charge-transfer complex molecules. Compounds I, II, III, IV, V, VI, and VII were synthesized with a 64-80 percent yield rate. Results from the investigation of the FT-IR, ¹H-NMR, and UV-visible Spectrophotometer in the current study are consistent with those from earlier studies in these subjects. Verifying that the predicted structures for each of the synthesized molecules are accurate. Regarding the theoretic inquiry, it may be concluded that the DFT (density functional theory) to be used in the investigation is a reliable technique, as well as B3LYP functional is an appropriate and effective method function to analyze the electronic properties of these molecular structures. The testing results were consistent with the 3-21G's geometrical characteristics (d, p). The electronic properties for compounds of charge-transfer complex are investigated in this work utilizing the density functional theory (DFT) method, together with geometry optimization using the functionals of B3LYP.

Total energies in addition to geometric structures (donor and acceptor,) systems showed how extremely stable the structures are. Additionally, as compared to other systems, the donor-acceptor system has a higher reactivity and an average polarizability. As a result of the study's findings, we are now able to choose the kind of bridge that will work with acceptor and donor to determine the physical characteristics of the acceptor, bridge, and donor.

Authors' declaration:

- Conflicts of Interest: None.
- We hereby confirm that all the Figures and Tables in the manuscript are mine ours. Besides, the Figures and images, which are not mine ours, have been given the permission for re-publication attached with the manuscript.
- Ethical Clearance: The project was approved by the local ethical committee in University of Thi-Qar.

Authors' Contribution Statement:

H. Sh. M. contributed in the design, acquisition of data, analysis, and the interpretation of the results. N. H. Al. contributed in the conception of the idea of the research, drafting the manuscript, revision and proofreading.

References:

1. Huang W, Xiao K, Luo L, Yang C, Ju Z, Chen J, Zhang J. Synthesis, structure, and charge transport properties of a novel donor-acceptor complex of coronene and DTTCNQ. *J Solid State Chem.* 2021 Aug 1; 300:122224.
2. Lee S, Hong J, Jung SK, Ku K, Kwon G, Seong WM, et al. Charge-transfer complexes for high-power organic rechargeable batteries. *Energy Storage Mater.* 2019 Jul 1;20: 462-9.
3. Liu G, Liu J, Dunn AS, Nadazdy P, Siffalovic P, Resel R, et al. Directional Crystallization from the Melt of an Organic p-Type and n-Type Semiconductor Blend. *Cryst Growth Des.* 2021; 21(9): 5231–9.
4. Chen Y, Li J, Gong J. Jumping crystal based on an organic charge transfer complex with reversible on/off switching of luminescence by external thermal stimuli. *ACS Mater Lett.* 2021; 3(3): 275–81.

5. Tayi AS, Shveyd AK, Sue AC-H, Szarko JM, Rolczynski BS, Cao D, et al. Tayi et al. reply Nature. 2017; 547(7662): E14–5.
6. Xu B, Li Z, Chang S, Ren S. Multifunctional molecular charge-transfer thin films. *Nanoscale*. 2019; 11(46): 22585–9.
7. Nakamura M, Horiuchi S, Kagawa F, Ogawa N, Kurumaji T, Tokura Y, et al. Shift current photovoltaic effect in a ferroelectric charge-transfer complex. *Nat Commun*. 2017 Aug 17; 8(1): 1-6.
8. Siegmund B, Mischok A, Benduhn J, Zeika O, Ullbrich S, Nehm F, et al. Organic narrowband near-infrared photodetectors based on intermolecular charge-transfer absorption. *Nat Commun*. 2017;8(1):1–6.
9. Ma C, Xu D, Wang P, Lin Z, Zhou J, Jia C, Huang J, Li S, Huang Y, Duan X. Two-dimensional van der Waals thin film transistors as active matrix for spatially resolved pressure sensing. *Nano Research*. 2021 Oct; 14(10): 3395-401.
10. Wang X, Wang W, Yang C, Han D, Fan H, Zhang J. Thermal transport in organic semiconductors. *J Appl Phys*. 2021 Nov 7;130(17):170902.
11. Fan ZP, Li XY, Purdum GE, Hu CX, Fei X, Shi ZF, et al. Enhancing the thermal stability of organic field-effect transistors by electrostatically interlocked 2D molecular packing. *Chem Mater*. 2018 May 21; 30(11): 3638-42.
12. Nath A, Asha KS, Mandal S. Conductive Metal-Organic Frameworks: Electronic Structure and Electrochemical Applications. *Chem. Eur J*. 2021 Aug 11; 27(45): 11482-538.
13. Prodanov M, Diakov M, Vashchenko V. A facile non-injection phosphorus-free synthesis of semiconductor nanoparticles using new selenium precursors. *Cryst Eng Comm*. 2020; 22(4): 786-93.
14. Sato R, Dogishi M, Higashino T, Kadoya T, Kawamoto T, Mori T. Charge-Transfer Complexes of Benzothienobenzothiophene with Tetracyanoquinodimethane and the n-Channel Organic Field-Effect Transistors. *J Phys Chem C*. 2017; 121(12): 6561–8.
15. Tanini D, Capperucci A. Ring opening reactions of heterocycles with selenium and tellurium nucleophiles. *New J Chem*. 2019; 43(29): 11451-68.
16. Rakitin OA. Fused 1, 2, 5-thia-and 1, 2, 5-selenadiazoles: Synthesis and application in materials chemistry. *Tetrahedron Lett*. 2020 Aug 20; 61(34): 152230.
17. Mohamed YM, Attia YA, Nazer HA, Solum EJ. An overview of recent development in visible light-mediated organic synthesis over heterogeneous photonanocatalysts. *Curr Org Synth*. 2021 Feb 1;18(1):23-36.
18. Ren Y, Xu B, Zhong Z, Pittman Jr CU, Zhou A. Synthesis of ArSe-Substituted Aniline Derivatives by C (sp²)-H Functionalization. *Asian J Org Chem*. 2018 Dec; 7(12): 2439-43.
19. Singh FV, Wirth T. Selenium Reagents for Organic Synthesis. *Curr Org Synth*. 2022 May 1; 19(3): 291-2.
20. Potts KT, Cody RD, Dennis RJ. Nonclassical heteropentalenes containing the selenodiazole, thiatriazole and selenotriazole ring systems. *J Org Chem*. 1981; 46(20): 4065–8.
21. Konstantinova LS, Rakitin OA. Chalcogen exchange in chalcogen–nitrogen π -heterocycles. *Mendeleev Commun*. 2021 Jul 1; 31(4): 433-41.
22. Sharma D, Arora A, Oswal P, Bahuguna A, Datta A, Kumar A. Organosulphur and organoselenium compounds as emerging building blocks for catalytic systems for O-arylation of phenols, a C–O coupling reaction. *Dalton Trans*. 2022; 51(21): 8103-32.
23. Młochowski J. Developments in the chemistry of selenaheterocyclic compounds of practical importance. *Phosphorus, Sulfur, and Silicon*. 2008 Apr 1; 183(4): 931-8.
24. Silverstein RM, Bassler GC. Spectrometric identification of organic compounds. *J Chem Educ*. 1962;39(11):546.
25. Wang K, Ran J, Wang F, Pan Z. Application of IR/SEM and other modern instruments for mineral identification. *Rock Miner Anal*. 2014; 33(5): 625–33.
26. Krupová M, Kessler J, Bouř P. Recent trends in chiroptical spectroscopy: theory and applications of vibrational circular dichroism and Raman optical activity. *Chem Plus Chem*. 2020 Mar; 85(3): 561-75..
27. Raheem AH, Al-Shejri KJ, Al-bermany ED. Density Functional Theory Calculations For MethylBenzene Molecules group. *Br J Sci*. 2012; 5: 57-64.
28. Salih NG, Obayes HR. Theoretical Study of [N]-Helicene Structure (N= 6, 12, 18, 24, 30, 36, 42, 48, 54) Using DFT. *Solid State Technol*. 2021; 64(2): 3909–19.
29. Wang X, Berkelbach TC. Excitons in solids from periodic equation-of-motion coupled-cluster theory. *J Chem Theory Comput*. 2020; 16(5): 3095–103.
30. Khuodhair AM, Ajeel FN, Oleiwi MO. Density functional theory investigations for the electronic and vibrational properties of donor-acceptor system. *J Appl Phys Sci Int*. 2016; 6(4): 202–9.
31. Kubba RM, Mohammed MA. Theoretical and Experimental Study of Corrosion Behavior of Carbon Steel Surface in 3.5% NaCl and 0.5 M HCl with Different Concentrations of Quinolin-2-One Derivative. *Baghdad Sci J*. 2022; 19(1): 0105-.
32. Kubba RM, Mohammed MA, Ahamed LS. DFT Calculations and Experimental Study to Inhibit Carbon Steel Corrosion in Saline Solution by Quinoline-2-One Derivative. *Baghdad Sci J*. 2021;18(1).
33. Sowlati-Hashjin S, Karttunen M, Matta CF. Manipulation of Diatomic Molecules with Oriented External Electric Fields: Linear Correlations in Atomic Properties Lead to Nonlinear Molecular Responses. *J Phys Chem A*. 2020; 124(23): 4720–31.
34. Kh S, Sh A, Mohammed L. Theoretical study for Coronene and Coronene-Al, B, C, Ga, In and Coronene-O interactions by using Density Functional theory. *Univ Thi-Qar J*. 2019;14(4): 80–94.
35. Abd El-Lateef HM, Shaaban S, Khalaf MM, Toghan A, Shalabi K. Synthesis, experimental, and computational studies of water soluble anthranilic organoselenium compounds as safe corrosion inhibitors for J55 pipeline steel in acidic oilfield

- formation water. Colloids Surfaces A Physicochem Eng Asp. 2021; 625: 126894.
36. Millefiori S, Alparone A. Second hyperpolarisability of furan homologues C₄H₄X (X= O, S, Se, Te): ab initio HF and DFT study. Chem Phys Lett. 2000; 332(1-2): 175-80.
37. Jabbar ML. Theoretical study for the interactions of Coronene-Y interactions by using Density functional theory with hybrid function. University of Thi-Qar Journal. 2018; 13(3): 28-41.
38. Hanoon FH, Jabbar ML, Alwan AS. Effect of thickness on the fractal optical modulator for MgF₂, LiF, Al₂O₃ materials by testing modulation transfer function (MTF). J Coll Educ Pure Sci. 2017; 7(4): 168-82.
39. Coropceanu V, Kwon O, Wex B, Kaafarani BR, Gruhn NE, Durivage JC, et al. Vibronic coupling in organic semiconductors: the case of fused polycyclic benzene-thiophene structures. Chem Eur J. 2006;12(7): 2073-80.

تحضير، تشخيص وإجراء دراسة نظرية لمعدقات انتقال الشحنة الجديدة المشتقة من N – فنيل -3,4- سيلينا داي ازو بنزو فينون امين

نهى حسين السعداوي

حيدر شنشول محمد

قسم الكيمياء، كلية العلوم، جامعة ذي قار، المثنى، العراق.

الخلاصة:

في الدراسة الحالية، تم استخدام طريقة مباشرة لإنشاء سلسلة جديدة من معدقات نقل الشحنة من المواد الكيميائية ذات حصرية جيدة، حيث تم إنتاج مركبات جديدة لمعدقات نقل الشحنة من خلال مفاعلة كينونات مختلفة كلا على حدة مع N- فنيل -3,4- سيلينا داي ازو بنزو فينون امين في مذيب الأستونيترييل بنسبة 1:1 مول وباستخدام تقنيات التحليل المعروفة مثل الأشعة فوق البنفسجية، والأشعة تحت الحمراء، و-¹H, ¹³C NMR، حيث تم تحديد جميع المواقع الفعالة للمركبات الناتجة حيث وجد انها تطابق نتائج التحليل للتراكيب الكيميائية المقترحة للمركبات المحضرة. بالإضافة الى ذلك تم استخدام نظرية الكثافة الوظيفية DFT لتحليل التركيب الجزيئي لمعدقات نقل الشحنة الناتجة من خلال استخدام برنامج الكاوسيين، حيث تم اكتشاف فجوة الطاقة الناشئة وأسطح HOMO و LUMO خلال عملية التحسين الهندسي باستخدام المجموعة الأساسية المكونة من 21G-3 من الهياكل الهندسية. كذلك تم تقييم الهندسة الجزيئية وخطوط المحيط للمركبات ذات معدقات نقل الشحنة أثناء التحسين الهندسي. كما تم التحقق أيضاً في الذرات المستقبلية والمانحة لمعدقات نقل الشحنة الناتجة من خلال مقارنة طاقات HOMO للمواد الكيميائية في معدقات نقل الشحنة. كذلك، تم حساب ودراسة الحالة الأرضية، والكهروسالبية، وجهد التأين، والكهروموجبية، والألفة الكهربائية.

الكلمات المفتاحية: معدقات نقل الشحنة، كينونات مختلفة، فجوة طاقة، طاقات الهومو، N-فنيل-3,4- سيلينا داي ازو بنزو فينون امين.